processes

MDPI

*Review*

# A Review of the Dynamic Mathematical Modeling of Heavy Metal Removal with the Biosorption Process

**Avijit Basu [1,*], Syed Sadiq Ali [1], SK Safdar Hossain [1] and Mohammad Asif [2]**

[1] Department of Chemical Engineering, King Faisal University, Al-Ahsa 31982, Saudi Arabia; ssali@kfu.edu.sa (S.S.A.); snooruddin@kfu.edu.sa (S.S.H.)
[2] Department of Chemical Engineering, King Saud University, Riyadh 11421, Saudi Arabia; masif@ksu.edu.sa
* Correspondence: abasu@kfu.edu.sa; Tel.: +966-59-409-1974

**Abstract:** Biosorption has great potential in removing toxic effluents from wastewater, especially heavy metal ions such as cobalt, lead, copper, mercury, cadmium, nickel and other ions. Mathematically modeling of biosorption process is essential for the economical and robust design of equipment employing the bioadsorption process. However, biosorption is a complex physicochemical process involving various transport and equilibrium processes, such as absorption, adsorption, ion exchange and surface and interfacial phenomena. The biosorption process becomes even more complex in cases of multicomponent systems and needs an extensive parametric analysis to develop a mathematical model in order to quantify metal ion recovery and the performance of the process. The biosorption process involves various process parameters, such as concentration, contact time, pH, charge, porosity, pore size, available sites, velocity and coefficients, related to activity, diffusion and dispersion. In this review paper, we describe the fundamental physical and chemical processes involved in the biosorption of heavy metals on various types of commonly employed biosorbents. The most common steady state and dynamic mathematical models to describe biosorption in batch and fixed-bed columns are summarized. Mathematical modeling of dynamic process models results in highly coupled partial differential equations. Approximate methods to study the sensitivity analysis of important parameters are suggested.

**Keywords:** biosorption; heavy metals; modeling; equilibrium; batch process; fixed-bed



**Citation:** Basu, A.; Ali, S.S.; Hossain, S.S.; Asif, M. A Review of the Dynamic Mathematical Modeling of Heavy Metal Removal with the Biosorption Process. *Processes* **2022**, *10*, 1154. https://doi.org/10.3390/pr10061154

Academic Editor: Andrea Petrella

Received: 16 May 2022
Accepted: 6 June 2022
Published: 8 June 2022



## 1. Introduction

Effective remediation of contaminants, especially heavy metals, from wastewater is a major emerging environmental challenge because of their adverse effects on human health [1–6]. Biosorption is a cost-effective remediation technique that is governed by both external and internal mass transport processes, in conjunction with surface forces, to immobilize pollutants from the fluid phase on to the active sites of the external surface and the internal matrices of the solid biosorbent [7]. This technique has been found to be highly effective in the removal of heavy metal ions, e.g., cobalt, lead, copper, mercury, cadmium, nickel, etc., from an aqueous phase [8]. Common methods of removing heavy metals have numerous drawbacks, including low efficiency and high costs. In biosorption, heavy metal removal is dependent on the active sites of the biosorbent [7]. Additionally, the use of highly porous, organic-based adsorbents for the remediation of highly toxic heavy metals from the aqueous phase inherits unique features, such as significant surface area, high chemical stability and the promotion of the reusage of adsorbents [1]. Experimental studies have been reported in the literature using a wide variety of biosorbents, such as protonated marine sargassum biomass, crab shells, chicken fat, coconut fiber, grape fruit biomass and fish scales [9–16].

Hence, it is essential to compile modules that validate experimental data with a transient concentration profile model in order to justify the elucidation of the sorption phenomenon

in a multicomponent bulk phase with respect to a heterogeneous substrate, such as a biosorbent. Thus, by modifying both the single-component isotherms and the dynamic column models, extended, multicomponent isotherms and dynamic column models can be utilized for scale-up procedures in order to optimize wastewater effluent treatment procedures. The significance of the heterogeneity of the adsorbent is addressed by quantifying the specific equilibrium coefficients of a specific ion's interaction with a specific functional group on the substrate. This approach helps in deducing generalized conclusions regarding the biosorption process, irrespective of the nature of the metal ion and the functional groups present on the substrate.

In short, the utility of a review on the quantification of pollutants in both bulk and adsorbed phases is essential to predicting the breakthrough characteristics of a fixed-bed dynamic column with respect to several contaminant ions in the bulk phase. The interfering ions may bear a profound impact on the adsorptivity of a specific ion in the bulk phase. Hence, with respect to EPA compliance standards, it is imperative to regulate the parameters, such as adsorbent dosage, pH of the bulk phase and the influent flowrate, for the optimization of the effluent concentrations of several species in conjunction with regulatory limits.

### *1.1. Biosorption Process*

Despite the fact that most industrial wastewater effluents are invariably contaminated with several metallic contaminants, most biosorption studies have focused on batch adsorption tests involving a single component [17]. During the biosorption of multispecies metal ions from an aqueous phase, several metal ions can simultaneously transport through the fluid phase and the competitively bind to the substrate (Figure 1). In most cases, empirical expressions, valid for mono-component biosorption, are simply extended to correlate the experimental data. However simple, this approach fails to provide a greater insight into the relative significance of various mass transport and adsorption mechanisms occurring simultaneously in the multicomponent biosorption process [18].

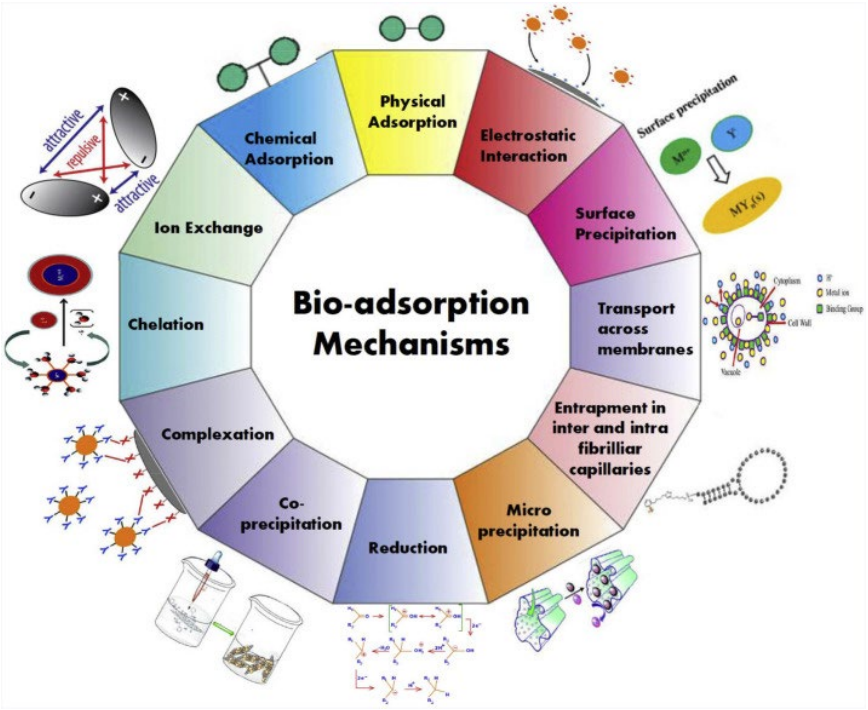


**Figure 1.** General mechanisms for heavy metal biosorption, adapted with permission from Ref. [19]. 2020, Elsevier.

The process of sorption with respect to a bioadsorbent can be summed up in three consecutive steps as follows:

(i) Diffusion of the contaminant ion from the bulk phase to the outer surface of the sorbent. The phenomenon of surface diffusion is accompanied by overcoming the mass transfer resistance offered by the double layer interface between the bulk phase and the outer surface of the adsorbent.
(ii) The surface diffusion is followed by diffusion of the ions from the outer surface of the adsorbent into its internal pores. In short, the pore diffusion is directly correlated with the internal porosity of the biomass. However, in some cases (e.g., microbial biosorbents), the sorption process occurs at the sorbent surface without this step.
(iii) Further, the interaction sites are available on the inner pore walls of the sorbent, and the chemisorption of the metal ions on the interaction sites of the substrate proceeds until they are completely saturated with the influent ions.

One of the several parameters that bears dominance in the overall adsorption behavior of the biomass is the mesoporous nature of the bioadsorbents. In other words, if the internal porosity of the packed bed in comparison to the external voidage is significant, the rate-limiting step of sorption kinetics in the internal walls of the pores is preceded by pore diffusivity. Under these underlying conditions, the concentration of pollutants in the pore phase can only be abated if the ionic size of the ion is equal or greater than the pore diameter. In addition, the distribution of the interaction sites with respect to internal pores and external surface also bears a profound effect on the overall adsorptivity of the pollutants. It has been observed that, with respect to dynamic adsorption in both batch and fixed-bed columns, the pH parameter is in a transient flux before attainment of the adsorption equilibrium. Hence, it has been noted that with changes in pH, the precipitation of metal ions (such as hydroxides) is prevalent. In brief, precipitations may lead to throttling of pores and external voids. This results in entrapment, which may attenuate the overall adsorption phenomenon.

### *1.2. Adsorption Isotherm*

Multicomponent adsorption is challenging since wastewater with several toxic pollutants requires the study of the competitive interaction among pollutants in the overall process [20]. Basu and Rahaman [21] have reported that the adsorption of a specific component in a multicomponent phase is dependent on interactive sorption coefficients with functional groups on the surface. In addition, the concentrations of each component in the bulk phase, pH of the bulk phase and the number of competitive interaction sites per unit mass of the adsorbent are other key parameters that characterize the sorption phenomenon. For the sake of simplicity, all the adsorption sites can be assumed to be equivalent, ignoring interactions on the adjacent sites of the adsorbent [22]. This assumption, however, needs to be carefully examined, since surface heterogeneity has been confirmed by spectroscopic methods in many biosorbents, such as fish scales and crab shells (Basu and Rahaman [23], Niu and Volesky [24]). For example, the molecular structure of fish scales exhibits the presence of amides and carbonyl groups, which provide specific binding site interaction and selectivity to specific metal ions [25]. Therefore, the overall removal of the contaminants is affected by the number of such specific interaction sites per unit mass of the adsorbent [26].

Thus, a comprehensive, multicomponent adsorption model requires usage of well-known, extended isotherm models, e.g., Langmuir and Freundlich, which incorporate single-component isotherms fitted to pure component data [27]. In addition, isotherms such as the Sips, Toth and Kahn isotherms can also be utilized as a hybrid of both the Langmuir and Freundlich isotherms in order to validate experimental data [20]. Research on the performance of adsorbent materials is essential for the design of equipment employing the adsorption process [28]. The analysis is usually performed via equilibrium studies on systems of interest. As the industry has not always opted for environmentally friendly solutions, biomasses used in dynamic column adsorption processes may require both efficient pretreatment and regeneration for further usage [29].

Activated carbon, because of its significant surface area per unit mass of the adsorbent, is one of the most commonly used adsorbents with respect to water purification. The process of activating the adsorbent promotes the creation of mesopores and as well as new and additional micropores in the material. These enlarged micropores initiate the efficient abatement of pollutants via the sorption process [30]. There are circumstances that intend to achieve a particular optimal pore distribution, where spatial homogenous pores within the particles are desired [31].

The equilibrium bulk phase solute concentration is reported in units of moles of the contaminant ion per liter of the bulk phase ($C$), while the amount of ions immobilized on the substrate is expressed as $Q$ in units of moles of the ions adsorbed per unit mass of the adsorbent. The relationship between the two quantities, i.e., $Q = f(C)$, is termed the "sorption isotherm" [32]. The validity of this relationship requires the establishment of the equilibria, while the physicochemical parameters, such as temperature, may vary or remain constant [33].

### 1.3. Uni-Component Adsorption Models

Different adsorption isotherm models have been discussed and categorized based on type of adsorption and the number of adjustable parameters (two, three, four and five parameter isotherm models) [34,35]. Thus, the isotherms can be classified as: (i) One-parameter isotherms, such as the relationship $Q = f(C)$ (both Langmuir and Freundlich models)—this is usually applicable when the adsorption process is initiated at low concentrations of the solutes in bulk phases—or (ii) two-parameter isotherms, such as the Hill–Debboer isotherm model, which incorporates mobile adsorption and lateral interactions among adsorbed molecules [36]. In addition, the Dubinin–Radushkevich and Temkin isotherms may be considered in order to address gaussian energy distribution in heterogeneous substrates and the effects of indirect adsorbate–adsorbate interactions, respectively [37,38]. A three-parameter isotherm, such as the Redlich–Peterson isotherm model, which validates a mixed model consisting of both the Langmuir and Freundlich isotherms, does not assume monolayer coverage [39]. A state-of-the-art review on adsorption isotherm models suggests that the process can be dependent on several parameters [40]. In addition, the accuracy of an isotherm model is generally a function of a number of independent parameters, while its significance in relation to the process application is indicative of its mathematical simplicity [41].

However, the sorption phenomenon is unique for each specific system and demands the utilization of several isotherm models. An explicit selection of an adsorption isotherm should adequately demonstrate the reaction mechanisms associated with the sorption process that may aid waste treatment projects at scaled-up design levels [42]. Linear regression analyses are often used to present the best fitting adsorption models to adequately quantify the correlation of concentrations of contaminants in both the bulk and adsorbed phases with justified assumptions [43].

Table 1 illustrates the significance of isotherms that provide an insight into modeling biosorption data with respect to the number of appropriate parameters.

Linear regression in data management is utilized to validate the experimental batch adsorption results. Due to its ease of quantification of experimental parameters (such as Langmuir coefficients), through the extensive application of linearized regressive models, linearized optimization has become an indispensable priority. However, in order to obtain significant coherent analysis of the experimental data, nonlinear isotherm models are also used with respect to biosorbents such as Chitosan [45] and wheat bran [46].

**Table 1.** A brief summary of the various isotherms applicable to modeling batch biosorption data.

| Isotherms | Equation | Applications | Parameters Involved |
|---|---|---|---|
| Langmuir [44] | $q_e = q_m K_a C_e (1 + K_a C_e)^{-1}$ | Homogeneous substrate. | 2 |
| Freundlich [44] | $q_e = K_F C_e^{\frac{1}{n}}$ | Heterogeneous substrates. | 2 |
| Hill–Debboers [36] | $\ln\left[C_e(1-\phi)\phi^{-1}\right] - (1-\phi)^{-1}\phi = -\ln(K_1) - \left(\frac{K_2\phi}{RT}\right)$ | Mobile adsorption. Interaction of adsorbed species. | 2 |
| Temkim [36] | $Q_e = \left(\frac{R_t}{b}\right)(\ln K_T + \ln C_e)$ | Indirect adsorbate/ adsorbate interaction. | 2 |
| Sipps [36] | $Q_e = \frac{K_s C_e{}^{bs}}{1 - a_s C_e{}^{bs}}$ | Heterogeneous substrates with high adsorbate concentration. | 3 |
| Redlich–Peterson [36] | $q_e = \frac{AC_e}{1+BC_e{}^{\alpha}}$ | Nonideal monolayer adsorption. | 3 |
| Kahn [36] | $Q_e = \frac{Q_{max} b_k C_e}{(1+b_k C_e)a_k}$ | Bioadsorption from pure dilute solutions. | 3 |
| Langmuir–Freundlich [36] | $q = \frac{Q_m (K_a C_{eq})^n}{1+(K_a C_{eq})^n}$ | Applicable to distribution of adsorption energy on heterogeneous substrates. | 3 |
| Dubinin–Radushkevich [36] | $Q_e = Q_m \exp(-Ke^2)$ $e = RT\ln\left(1 + \frac{1}{C_e}\right)$ | Non-isothermal conditions. | 3 |

### *1.4. Biosorption Kinetics Mechanism*

Significantly, the sorption kinetics mechanism is dependent on the concentration of ions, the pore size of substrate, the pH of the bulk phase and the number of binding sites per unit mass of the adsorbent.

Smaller pore sizes often lead to the dominance of smaller-sized ions by excluding ions with higher ionic radii. In addition, the pore diffusivity of the contaminant is directly proportional to the internal porosity of the adsorbent, and inside the internal walls of the substrate, the binding sites are available. The sorption of these contaminant ions is preceded by the diffusion of contaminants within the pore walls of the substrate [21]. Overall, the rate of reaction is a function of both the kinetics of sorption and desorption, and at equilibrium conditions, the rate of adsorption is equal to the rate of desorption. Hence, a dynamic equilibrium is established at the steady state concentration of the bulk phase. Thus, it is of extreme significance to consider the above parameters in assuring a highly efficient removal of ionic contaminants with both ion exchange mechanisms and electrostatic forces. The mechanisms associated with biosorption can include complexation, precipitation reactions with ion exchange and electrostatic attractions [47].

The attributes that determine adsorption efficiency are porosity and the pore size of adsorbents and their surface area [48]. Overall, model equations are usually solved via the application of parameters such as pore diffusivity (internal diffusion coefficient) and surface diffusivity (external diffusion coefficient) [49].The rate-controlling step is correlated to either the ionic or the molecular diffusion of the contaminant from the bulk phase to the inner internal walls of the substrate. The driving force that initiates the diffusion of a specific contaminant is its concentration gradient between the two phases. This driving force has to overcome the resistance due to the film encapsulating the substrate and inner pore walls. The film that resists the diffusivity between the bulk and adsorbed phases is a thin layer of constant thickness that behaves as the interphase between the two phases. It is assumed that the thickness of this film remains constant throughout the sorption phenomenon [50,51]. Additionally, the sorption process depends not only on the driving force but also on the specific number of vacant sites and their corresponding interactive affinity coefficients with respect to each specific ion. Electronegativity and the atomic weight of metals can play a significant role in the quantification of affinity coefficients with

respect to multicomponent adsorption. It has been validated that competition between two metal ions for a specific site is advantageous for a metal with lower electronegativity and higher atomic weight values [52]. Dissanayake et al. [53] reported that adsorbents such as *Asplenuim nidus* have demonstrated that lead ions (atomic weight 208) bear a higher adsorption capacity when compared to nickel (atomic weight 58). However, the dilemma is that, with increasing atomic weight, ionic size increases, and its pore diffusivity is increasingly hindered with adsorbent particles bearing decreasing pore sizes. Recently, using a nonlinear mathematical model to describe pore diffusion in polymers (which may include biosorbents) has been proposed. The model can be formulated by assuming that the diffusing ion causes a deformation that induces a viscoelastic stress responsible for a convective field. This convective field is defined as representing an opposition to the concept of Fickian diffusion [54].

In retrospect, we can conclude that adsorbents with heterogeneous sites, each possessing specific interaction coefficients, have separate binding affinities with specific ions in a multicomponent phase. The selectivity of each contaminant ion is severely affected by the presence of competing ions in the bulk phase and is dependent on factors such as electronegativity and the atomic sizes of each ion, number and interaction coefficient of specific sites in the substrata and pH of the bulk phase, which acts as a competing hydronium ion. Simultaneously, at pH values lower than the zero-point charge of the adsorbent (zpc), electrostatic repulsive forces will aid adsorption delay. Some examples of the applications of biosorption models for well-known biosorbents are listed below in Table 2.

**Table 2.** Examples of biosorption kinetics on specific bioadsorbents.

| Applied Reaction Kinetics Model | Biosorbent | Reference |
|---|---|---|
| Pseudo-second-order | Typha domingensis leaf powder | Ghani et al., 2009 [55] |
| Pseudo-second-order | Carbonaceous adsorbent from black liquor sludge | Sari et al., 2017 [56] |
| Pseudo-second-order | Base-treated ber (Hevea brasiliensis) | Ngah and Hanafiah, 2008 [57] |
| Pseudo-second-order | Bacillus Badius AK | Vishan et al., 2019 [58] |
| Pseudo-first-order | Biochar | Du et al., 2016 [59] |
| Pseudo-first- and second-order | Fungal Cell | Lu et al., 2020 [60] |

## 2. Batch Models

### *2.1. Multicomponent Equilibrium Models*

#### 2.1.1. Isotherm Models

A sorption isotherm is often assumed to be constructed from data obtained at reaction equilibrium. In that case, the adsorption isotherm (made from measurements of progressive adsorption up to the equilibrium) should be the same as the desorption isotherm (made from measurements of progressive release into the solution up to the equilibrium) because the theory of thermodynamic equilibria assumes a complete reversibility of the chemical reactions and, thus, a unique ($c$, $q$) pair [32].

Overall, understanding and quantifying the multicomponent modeling of metal ions on biosorbents at equilibrium conditions are imperative to scaled-up design procedures for dynamic column runs. Calculations with respect to batch isotherms are dependent on explicit models based on Langmuir, Freundlich, BET and other isotherms. In addition, extended Freundlich–Langmuir models are often utilized for design calculations [27]. Langmuir and Freundlich isotherms, coupled with pseudo-first-order and second-order models with intra particle diffusion, can be applied to experimental data to check the effectiveness of the abatement process [61]. For a single-component system, the Batch equilibrium data can be represented as [62]

$$q_e = \frac{C_0 - C_e}{W} \quad (1)$$

For a multicomponent species of value $i$ = 1, 2,3, . . .

The above equation is modified as:

$$q_{e,i} = \frac{C_{0,i} - C_{e,i}}{W} \quad (2)$$

Mohan and Singh [63] have observed that the mutual effects of metal ions in a multicomponent phase can be determined by calculating the ratio of the adsorption capacity of the metal ions in the multicomponent phase to the ratio of the adsorption capacity in the single-component phase ($q_i{}^{mix}/q_i$). If the ratio is less than unity, the metal ion competes with the co-ions for adsorption in the substrate. It is noteworthy to mention that sensitivity analyses of the adsorption of ions interferes with the concentration of the hydronium ion as dictated by the pH of the bulk solution. Additionally, Yorrik et al. [64] have reported that, with respect to initial higher concentrations of the metal ion, the corresponding pseudo-first-order reaction simulations reasonably validate the experimental data. Similarly, at lower initial effluent concentrations, the pseudo-second-order kinetic models do comply with the experimental data.

Biosorbents are heterogenous in nature and often consist of several functional groups [23]. Hence, it is imperative to define the equilibrium interactions of a contaminant ion with respect to a specific functional group on the surface of an adsorbent. The latest citations indicate that researchers have largely considered IAST, or Ideal Adsorbed Solution Theory, for modeling batch equilibrium data. In an Ideal Adsorbed Solution system, the modified [65] model quantifies the multicomponents in a bulk phase in correlation with Raoult's law. The IAST model has the distinct advantage of coupling single-component adsorption equilibrium data into a multicomponent bulk phase. In short, the presence of interfering or competing ions and their relative concentrations is largely neglected in calculating equilibrium data for each specific component [66].

Often, the design of the adsorption system depends on adsorption isotherms that could be satisfactorily fitted to experimental equilibrium adsorption data. Several adsorption isotherms are available to compute equilibrium data. Therefore, batch adsorption methods depend on multicomponent equilibrium adsorption data. These data are more difficult to procure than single-component adsorption data [67].

A comprehensive description of the IAST models, with respect to parameters such as temperature and pressure, are as displayed in Equations (3)–(5) [68]:

$$x_{e,i} = \frac{q_{e,i}}{q_T} \quad (3)$$

For an ideal solution system, the equation can be expressed as:

$$\frac{1}{q_T} = \sum_{i=1}^{N} \frac{X_{e,i}}{q_i{}^0} \quad (4)$$

$$\psi_1 = \psi_2 = \psi_3 =, \ldots, = \psi_i \quad (5)$$

where

$\psi$ = spreading pressure for individual components;
$q_{ei}$ = adsorbed phase concentration of species I (mmol per unit mass of adsorbent);
$q_i{}^0$ = adsorbed phase concentration of single-component $i$ (mmol per unit mass of; adsorbent;
$q_T$ = total amount of species adsorbed (mmol per unit mass of adsorbent).

The IAST utilizes thermodynamic approaches to describe the multicomponent adsorption isotherm with single-component adsorption data. The IAST is based on the assumption that the adsorbed mixture forms an ideal mixture at a constant spreading pressure and can be expressed as [69]:

$$\Pi = \Pi_1 = \frac{RT}{A} \int_0^{C_{e,i}{}^*} \frac{q_{ei}}{C_{e,i}} dC_{e,i} \quad (6)$$

$\Pi$—spreading pressure of system;
$\Pi_i$—spreading pressure of each component $i$;
$R$—universal gas constant;

$T$—temperature in K;
$A$—external surface area per unit mass of adsorbent.

where $C^0{}_i$ ($\pi_i$, $T$) is the equilibrium liquid-phase concentration of pure solute, $i$, at the same temperature, T, and spreading pressure, $\pi_m$, of the mixture with N components.

It is imperative to note that modifications to IAST model are indispensable for adequate representations of specific adsorption systems [69]. Several similar models, presented in Table 3, consist of specific isotherms that bear significance with multicomponent batch sorption data.

**Table 3.** A brief list of multicomponent Langmuir and Freundlich models.

| Model | Expression | Reference |
|---|---|---|
| Multicomponent Langmuir Isotherm | $q_{e,i} = \frac{q_m b_i C_{e,i}}{1+\sum_i^N b_i C_{e,i}}$ | [70] |
| | $q_1 = \frac{n_1 R_{sm} K_1 C_1^{n_1}}{1+K_1 C_1^{n_1}+K_2 C_2^{n_2}}$, $q_2 = \frac{n_2 R_{sm} K_2 C_2^{n_2}}{1+K_1 C_1^{n_1}+K_2 C_2^{n_2}}$ $K_1 = \frac{[R_S M_{1n_1}]}{[M_1]^{n_1}[R_S]}$, $K_2 = \frac{[R_S M_{2n_2}]}{[M_2]^{n_2}[R_S]}$ | [71] |
| Langmuir kinetic with competition between $n$ species | $\frac{dQ}{dt} = \frac{\theta}{\rho} k_{1,i} C_i \left( Q_{max} - \sum_{j=1}^{n} Q_j \right) - k_{-1,i} Q_i$ | [71] |
| Multicomponent Langmuir–Freundlich | $q_{e,i} = \frac{q_m b_i (C_{e,i})^{k_i}}{1+\sum_i^N b_i (C_{e,i})^{k_i}}$ | [71] |

It has been observed that acid base titration data can be concluded from Equations (6) and (7) to quantify, respectively, the intrinsic equilibrium coefficients ($K_1$ and $K_2$ in Table 2) and the number of specific interaction sites available per unit mass of the adsorbent.

$$\frac{1}{[H^+]} = \left(\frac{N_S}{K_1{}^{\text{int}}}\right)\left(\frac{1}{S^- H^{2+}} + \frac{1}{K_1{}^{\text{int}}}\right) \quad (7)$$

$$[H^+] = \left(N_S K_2{}^{\text{int}}\right)\left(\frac{1}{S^-}\right) - K_1{}^{\text{int}} \quad (8)$$

The intrinsic acidity $K_1^{\text{int}}$ and $K_2^{\text{int}}$ (acidic intrinsic coefficients) and $N_s$ (total number of sites per unit mass of the adsorbent) can be determined from the slopes and intercepts of Equations (5) and (6) [72]. The pH value of the bulk phase is recorded after each addition of the appropriate reagent. The total amount of adsorption of protons or hydroxyl ions to the substrate is correlated to $S^-$ or $S^- H^{2+}$ molar concentrations [23]. However, it has been observed that Equations (6) and (7) are equated with apparent constants, and the objectivity of the determination of several metal species (in a multicomponent phase) at multiple pH values is accomplished by determining the total number of both sites and functional groups per unit mass of the substrate [23].

However, these models (Equations (6) and (7)) are fitted with apparent constants. In general, the objective function for the model simulation is to determine the uptake of lead and arsenic ions (bicomponent) at various pH levels. This is achieved by determining the total number and types of sites per unit mass of the adsorbent. It is easily inferable at this stage is that bioadsorbents consist of several functional groups, and the equilibrium constant between a specific ion I bulk phase is distinctly correlated with a specific functional group. Thus, the total uptake of a specific ion with respect to a specific functional group is dependent on the concentration of the competing ions besides pH and the specific concentration of metal ions in the bulk phase. In order to determine the zero-point charge of the adsorbent, the logarithmic values of the acidity constants from Equations (6) and (7) are correlated to determine the zero-point charge of the adsorbent using Equations (8)–(10) [23].

$$pk_1{}^{\text{int}} = -\log K_1{}^{\text{int}} \quad (9)$$

$$pk_2{}^{\text{int}} = -\log K_2{}^{\text{int}} \tag{10}$$

$$P_{zpc} = \frac{\left(pk_1{}^{\text{int}} + pk_2{}^{\text{int}}\right)}{2} \tag{11}$$

Batch adsorption data with respect to a multicomponent phase are conducted at various pH levels, and the objective of the investigations is to determine the ultimate adsorption capacities of each ionic component. Because the Langmuir equation describes adsorption in a homogeneous substrate, Gaussian energy distribution is utilized to adjust monolayer adsorption on a heterogeneous substrate, such as a bioadsorbent [73].

The metal-adsorbing capability of various kinds of biomass adsorbents can be dependent on metal ions and parameters such as the nature of the biomass, composition of the bulk phase and, in addition, the preparation and physicochemical pretreatment of the biomass [74]. The Langmuir isotherm in its multicomponent phase has been extensively utilized for the quantification of biosorption processes with respect to contaminant ions in an aquatic bulk phase. It has been reported that the Langmuir isotherms of several competing ions are correlated to an ion exchange mechanism with a specific functional site on the substrate of a bioadsorbent [75]. Cations such as lead (unlike anions) are adsorbed both in the immobile phase and with functional groups, such that lead ions do replace calcium ions via ion exchange mechanisms in biomasses such as bones [76]. Consequently, it has been validated that cation uptake is relatively higher than anionic immobilization [77].

However, the interpretation of parameters for the Langmuir model is of questionable value since the number of binding sites in the biomass do not actually change with pH [26]. At low pH values in the bulk phase, a significant number of binding sites per unit mass of the adsorbent are protonated. Hence, one of the major assumptions of biosorption modeling studies is that the total number of available binding sites for a metallic ion is independent of the pH of the bulk phase in transient conditions [78]; this is a serious limitation in modeling.

Often, batch adsorption data consists of multicomponent ions in varying concentrations in a bulk phase. Assuming that the adsorption of a specific species is independent of the presence of several competing ions, the Langmuir adsorption isotherms can be documented [79]:

$$W_1 = \frac{Q_{m,1} d_1 C_{e,1}}{1 + d_1 C_{e,1}} \tag{12}$$

$$W_2 = \frac{Q_{m,2} d_2 C_{e,2}}{1 + d_2 C_{e,2}} \tag{13}$$

Using indices 1, 2 and 3 to $n$, the number of species in the bulk phase, Equation (11) is modified.

Expressing $W_2$ is a function of the initial and equilibrium concentrations, then

$$\frac{1}{W_1} = \left(\frac{1}{Q_{me,1}}\right) + \left(\frac{1}{Q_{me,1} d_1 C_{e,1}}\right) \tag{14}$$

As such, Equations (11) and (12) can be linearized, and values of $d$ (Langmuir coefficient for each specific species) can be determined as:

$$W_2 = \frac{C_{0,2} - C_{e,2}}{w} \tag{15}$$

$d$ is the Langmuir coefficient of a species (L/mmol);
$w$ is the amount of adsorbent per liter of solution (g/L);
$W$ is the amount of contaminant adsorbed per unit mass of the adsorbent (mg/g);
$C_e$ is the equilibrium concentration of a contaminant in the bulk phase (mmol/L);
$Q_m$ is the maximum adsorption capacity of a species (mg/g).

Solving Equations (12) and (13) simultaneously,

$$d_2 = \frac{(C_{o,2} - C_{e,2})(1 + d_1 C_{e,1})}{(Q_{m,2} W + C_{e,2} - C_o) C_{e,2}} \quad (16)$$

The Langmuir isotherm is the most widely used adsorption isotherm for the sorption of solutes from an aqueous bulk phase. The dominant ion exchange mechanism can be interpreted as [80]:

$$q_{e,i} = \frac{q_{m,i} K_{L,i} C_{e,i}}{1 + \sum_{i=1}^{n} K_{L,i} C_{e,i}} \quad (17)$$

where $q_e$ is the equilibrium amount of metal ions adsorbed in mg/g, $q_m$ is the total maximum amount of metal ions adsorbed in mg/g, $C_e$ is the total equilibrium metal ion concentration in mg/L and $K_L$ is the Langmuir constants showing the maximum adsorption capacity and affinity of the binding sites and the energy of adsorption in L/mg. $i$ represents the specific species, I and n are the number of species in the bulk phase.

However, it must be appreciated that Equation (16) bears a serious limitation with respect to biosorption. The metal ions represented in the above equation are correlated to a generalized Langmuir constant, $K_{L,I}$, by assuming that the adsorbent is homogeneous in nature.

The experimental values of $q_e$ and $C_e$ are initially treated with linearized equations in order to determine the model's parameters, and the isotherms are reconstituted using the determined values [81]. The researchers report that isotherm plots reveal the validation of experimental data (points) via simulated results (lines). Further, it has been observed that linear correlation coefficients ($r$) invoke the fit between experimental data and the linearized forms of isotherm equations, while the average percentage errors (APE) calculated according to Equation (17) indicate the fit between the experimental and predicted values of adsorption capacity used for plotting isotherm curves:

$$APE\% = \frac{\sum_{i=1}^{N} \left| (Q_e)_{experimental} - \frac{(Q_e)_{predicted}}{(Q_e)_{experimental}} \right|}{N} \times 100 \quad (18)$$

A multicomponent isotherm for one binding site, and the formation of 1:1 complexes (adsorbate/adsorbent) has been reported [82]. These isotherms are adapted in the cases of both multi-ion and multi-sites with several ion valences. A combination of chemisorption and ion exchange mechanisms reveals the equation of the cation, $M$, of the charge, $j$, adsorbing to a binding site, $B$, as:

$$jB^- + M^{j+} \rightleftharpoons j\left(M_{1/j}B\right) \quad (19)$$

$$K_{MB} = \frac{\left[M_{1/j}B\right]^j}{[M^+][B]^j} \quad (20)$$

Assuming all activity coefficients are equal to unity (under ideal solution behavior), the subscript, $MB$, on the left-hand side of the equation refers to the binding site with respect to cation $M$. The left term, $K_{MB}$, in the above equation is defined as the equilibrium constant of species $M$ with respect to with respect to site type $B$. The term $M_{1/j}B$ has been selected in substitution for $MB_j$, which signifies that a number of bonds equal to charge j of the cation have to be broken for the release of a $j$ valent ion [42]. Thus, the disassociation reaction is of order $j$ and not of the order of unity, as would be the case of a $MB_j$ species [42]. Accordingly, the former version should be preferred over the latter if the ion exchange complexation mechanism is dominant over the nonspecific electrostatic attraction between the ion and the binding site. In addition, it is assumed that secondary interactions such as electrostatic attractions (and/or repulsions) and hydrogen bonding are insignificant and that there is no other influence from other cations apart from competition for the same binding sites [26]. The researchers propose that, for the reaction of ion $M_j$+ in a system with n number of species and m binding sites, the following model can be quantified as:

$$W = \sum_{k=1}^{m} \left[ {}^{j}M_{1/zj}{}^{k}B \right] = \sum_{k=1}^{m} {}^{kt}B \frac{\left( {}^{kj}K\left[ {}^{j}M \right] \right)^{1/zj}}{1 + \sum_{h=1}^{n} \left( {}^{kh}K\left[ {}^{h}M \right] \right)^{1/zh}} \quad (21)$$

The binding sites in a bioadsorbent, such as Atlantic codfish scales with respect to lead and arsenic ions [21], are assumed to be predominantly composed of carbonyl (signified by C) and amide groups (signified by *S*) [23]. The model also includes two sites, the ${}^{t}C_a$ and ${}^{t}Ph$ groups (carbonate and phosphorous), for arsenic adsorption. Thus, Equation (19) can be further modified as follows:

$$W(Pb) = \left[ \frac{{}^{t}C\left( {}^{C1}K\left[ {}^{1}M \right] \right)^{1/2}}{\left(1 + {}^{CH}K[H]\right) + \left( {}^{C1}K[{}^{1}M] \right)^{1/2} + \left( {}^{C2}K[{}^{2}M] \right)^{-1/1}} \right] + \left[ \frac{{}^{t}S\left( {}^{S1}K\left[ {}^{1}M \right] \right)^{1/2}}{\left(1 + {}^{SH}K[H]\right) + \left( {}^{S1}K[{}^{1}M] \right)^{1/2} + \left( {}^{S2}K[{}^{2}M] \right)^{-1/1}} \right] \quad (22)$$

$$W(As) = \left[ \frac{{}^{t}C_a\left( {}^{C2}K\left[ {}^{1}M \right] \right)^{-1}}{\left(1 + {}^{CH}K[H]\right) + \left( {}^{C1}K[{}^{1}M] \right)^{1/2} + \left( {}^{C2}K[{}^{2}M] \right)^{-1}} \right] + \left[ \frac{{}^{t}Ph\left( {}^{S2}K\left[ {}^{2}M \right] \right)^{-1}}{\left(1 + {}^{SH}K[H]\right) + \left( {}^{S1}K[{}^{1}M] \right)^{1/2} + \left( {}^{S2}K[{}^{2}M] \right)^{-1/1}} \right] \quad (23)$$

[*H*] + b [*M*] = constant, where *b* is the valence of the metal ion (charge balance).

The relative spontaneity of a biosorption process is correlated to the thermodynamic parameters of the Gibbs free energy change, $\Delta G^0$. Gibbs free energy change ($\Delta G$) values can discern whether a process is spontaneous or not, and the negative values of $\Delta G$ imply a spontaneous process [10]. In addition, negative values of $\Delta G^0$ for a corresponding metal ion confirm the feasibility of the process and the spontaneous nature of the bioadsorption [83]. The researchers report that the values of $\Delta G^0$ were observed to increase from −26.24 to −29.66 kJ/mol for lead ion biosorption and from −18.66 to −21.2 kJ/mol for copper ion biosorption as the adsorbate solution temperature increased from 299 to 329 K. Thus, $\Delta G^0$ is negative, since the energy of the system decreases during the reaction to reach a more stable state [32].

The relation between $\Delta G^0$ and the reaction constant *K* (dimensionless) is provided by Equation (18) [84]:

$$K = e^{\frac{-\Delta G^0}{RT}} \quad (24)$$

where [85]:

$$\Delta G^0 = -RT \ln(K_C)$$

$$K_C = {}^{q_e}/_{C_e}$$

In addition, thermodynamic equilibrium is the result of competition between two contrary mechanisms, represented by the activation energy of adsorption, $E_1$, and desorption, $E_{-1}$.

The Arrhenius law (Equation (19) provides the relationship between the kinetic constants, *k* (dimensionless), and the activation energy, *E* (J mol$^{-1}$) [84]:

$$K = De^{\frac{-E}{RT}} \quad (25)$$

*D* is a dimensionless collision probability factor.

Hence, the relationship between the reaction energy of the reaction and the activation energies is:

$$\Delta G^0 = E^1 - E^{-1} \quad (26)$$

Thus, *K* can be interpreted as:

$$K = {}^{K_1}/_{K_2} \quad (27)$$

It can be concluded that not only can a reaction can be thermodynamically spontaneous ($\Delta G^0$ negative, $K > 1$), it can also be (i) fast, either for adsorption or desorption (low $E_1$ and low $E_{-1}$), (ii) slow for desorption (high $E_{-1}$) or even (iii) slow for adsorption and desorption (high $E_1$, higher more $E_{-1}$) [32]. Incorporating these intrinsic values in a software package will aid in the properly elucidating the reaction steps of the metal ion with respect to a specific binding site on the substrate.

Overall, by utilizing the isotherm models, the amount of metal ion adsorbed per unit mass of the adsorbent can be calculated as $X$. The predicted $X$ values are compared with the measured ones (actual values) by plotting the predicted $X$ (from the isotherm) vs. the measured $X$ in the $XY$ coordinate system [12]. A linearized plot of the inverse of the equilibrium concentration in the bulk phase vs. the inverse of the amount of metal ions adsorbed per unit mass of the adsorbent assists in determining the slope and intercept of the plot. Further, software packages may consider the significance of the porosity of a bioadsorbent and calculate the coefficients of each specific run [86].

#### 2.1.2. Pore Diffusion Model

In correlation to the models introduced in Table 2, it has been reported that the adsorption capacity of a metal ion is enhanced by increasing the pore size of an adsorbent [87]. However, after reviewing the above models, it can be concluded that the concept of internal porosity in an adsorbent has been ignored in the quantification process. The concept of porosity in correlation to adsorption mechanisms is a DUAL POROSITY concept that incorporates external voidage and internal porosity [21].

The researchers propose a three-way partition of the porous medium that includes (a) a solid phase, (b) a pore phase and (c) a bulk phase. At lower internal porosity conditions, the pore diffusivity of a cation (with respect to a larger atomic weight, such as in lead ions) is significantly limited. However, simultaneously (for ionic diameters less than the throat diameter of the pore), it can be concluded that the diffused ion in a mitigated pore diameter is highly susceptible to attenuation at its inner substrate due to a reduced distance between the interactive forces. The ratio of the internal porosity to external voidage is directly proportional to the adsorptivity of the ion. Thus, the rate of mass transfer between the bulk phase and the external substrate of the sorbent is proportional to the concentration gradient existing between the two phases. The equation describing the phenomenon was first stated by $cm^2/h$ [21]:

$$\left(D_p\rho\frac{1}{(1-x_i)}+\rho_a\frac{D_s}{\alpha}\frac{d\omega_i}{dx_i}\right)=k_{fi}(y_i-x_{si}) \tag{28}$$

where $w_i$ is the mole of ion $i$ adsorbed per unit mass of the adsorbent, pa is the density of adsorbent ($g/cm^3$), $p$ is the density of solution (g $mol/cm^3$), $k_{fi}$ is the mass transfer coefficient of component $i$ at the substrate of the pellet, (g mol/cm/h), $x_{si}$ is the mole fraction of component $I$ at the outer surface of the adsorbent at any time $t$, $x_i$ is the mole fraction of component $i$ in the pore phase, $y_i$ is the mole fraction of component I in the void phase, $D_p$ ($cm^2/h$) is the pore diffusivity of the effluent and $D_s$ ($cm^2/h$)is the surface diffusivity of the effluent.

In addition, dynamic equilibrium is when ions in the adsorbed phase bear a direct correlation to the ions in the pore phase. This adsorbed phase includes the already occupied sites by the sorbate at earlier time intervals. In other words, when the sites become saturated with ions, further immobilization of the ion on the internal walls of the substrate is terminated.

Hence, the ions in the adsorbed phase are expressed as:

$$V_i=x_i\left(\frac{\alpha}{\varepsilon}\right)V_{vi}+y_iV_{vi}+W_i \tag{29}$$

or

$$V_i=x_iV_{vi}\left(\frac{\alpha}{\varepsilon}+1\right)+W_i \tag{30}$$

where $W_i$ is the total volume of contaminants adsorbed in the pore phase.

The isotherms relating $w_i$ and $x_i$ are interpreted as:

$$w_i=\left(\frac{1-\varepsilon}{\rho_a}\right)\left[(Q_md-1)\rho x_i-d\rho^2x^2\right]\frac{1}{(1+d\rho x_i)} \tag{31}$$

where

$Q_m$ is the maximum adsorption capacity of a species (mg/g);
$d$ is the Langmuir coefficient (L/mmol);

If $x$ is insignificant, $x^2$ will be negligible.

$$w_i = \left(\frac{1-\varepsilon}{\rho_a}\right)\left[(Q_m d - 1)\rho x_i - d\rho^2 x^2\right]\frac{1}{(1+d\rho x_i)} \tag{32}$$

The pore diffusion model for multicomponent ions on a bioadsorbent bearing several functional groups in its substrate neglects the effects of secondary interactions, such as electrostatic bonding and hydrogen bonding. The dominant mechanism is a competition of various ions in the pore phase for the same binding site. With respect to the chemisorption of ion $M_j^+$ in a system with $n$ cations and $m$ binding sites, an expression in generalized form can be documented as:

$$w = \sum_{k=1}^{m}\left[M_{i/j}B\right] = \frac{\sum_{k=1}^{m} B^t K_{MB}[M]^{i/j}}{\sum_{h=1}^{n} K_{MB}[M]^{i/j}} \tag{33}$$

For simulation procedures, a contaminant phase consists of $n$ types of ions. If the biomass of several binding sites, ${}^tC$ and ${}^tS$, and $n$ = 1, 2. [H$^+$], is the hydrogen ion concentration and a measure of the pH of the bulk phase, and X is the mass of adsorbent in the bulk phase, then, in relation to first species, $n$ = 1

$$\begin{aligned} W(Pb) &= X^tC\left({}^{C1}K\left(\left[{}^1M\right]\right)^{1/2}\right)\times\frac{1}{\left(1+{}^{CH}K[H]+{}^{C1}K\left(\left[{}^1M\right]\right)^{1/2}+\left({}^{C2}K\left[{}^2M\right]^{-1/1}\right)+\left({}^{C3}K\left[{}^3M\right]^{1/2}\right)\right)} \\ &+X^tS\left({}^{S1}K\left(\left[{}^1M\right]\right)^{1/2}\right)\times\frac{1}{\left(1+{}^{SH}K[H]+{}^{S1}K\left(\left[{}^1M\right]\right)^{1/2}+\left({}^{S2}K\left[{}^2M\right]^{-1/1}\right)+\left({}^{S3}K\left[{}^3M\right]^{1/2}\right)\right)} \end{aligned} \tag{34}$$

In relation to the second species, $n$ = 2

$$\begin{aligned} W(As) &= \frac{X^tC\left({}^{C2}K\left[{}^2M\right]^{-1}\right)}{\left(1+{}^{CH}K[H]+{}^{C1}K\left[{}^1M\right]^{1/2}+{}^{C2}K\left[{}^2M\right]^{-1/1}+{}^{C3}K\left[{}^3M\right]^{1/2}\right)} \\ &+\frac{X^tS\left({}^{S2}K\left[{}^2M\right]^{-1}\right)}{\left(1+{}^{SH}K[H]+{}^{S1}K\left[{}^1M\right]^{1/2}+{}^{S2}K\left[{}^2M\right]^{-1/1}+{}^{S3}K\left[{}^3M\right]^{1/2}\right)} \end{aligned} \tag{35}$$

The maintenance of the neutrality of the solution is obtained in both the internal pore phase and voidage by assuming a constant charge balance at a specific time, $t$, and is represented as:

$$[OH] + b[M] = [H] + a[N] \tag{36}$$

Overall, it is noted by Basu and Rahaman [21] that the effective pore and surface diffusivities are non-Fickian by nature. The values of $d_1$ and $d_2$ are calculated based on batch adsorption tests. Further, this data is coupled into the code for simulation in dynamic column runs. Non-Fickian diffusion is the dominant mechanism with respect to biosorption. It has been reported that pore diffusivities are sensitive to ionic radii and the microstructure of the adsorbent. Often, the pore size of the adsorbent contributes to the rate-limiting step with respect to the mobility of the ion in the bulk phase. Constricted pore size distributions in Chitosan (a bioadsorbent) have significantly contributed to pore diffusivity fluctuations [88].

### *2.2. Models for Sorption Kinetics*

These models can be effectively coupled into dispersion-based mass transfer formulations to define sorption rates quantitatively. The researchers stress the importance of selecting a simple model based on a mechanistic knowledge of the system that can be upgraded to an advanced form by introduction of appropriate physical parameters (if required). However, it is imperative to justify the upgraded model by preceding it with the validation of the experimental data.

2.2.1. Single-Component Pseudo-First- and Second-Order Models

The kinetics of adsorption elucidate the variance in the abatement of specific metal ions from the bulk phase, with respect to the time interval and its parameters, on a substrate of the adsorbent. Some of the well-known equilibrium isotherms are presented in Table 4. Additionally, the design of a bioadsorption process is significantly dependent on kinetic models [80]. The researchers state that pseudo-first-order and second-order reaction models are extensively used as kinetic models to validate bioadsorption processes. The pseudo-first-order kinetic model is:

$$q_t = q_e(1 - e^{-k_1 t}) \tag{37}$$

The linear form of the pseudo-first-order kinetic model is:

$$\ln(q_e - q_t) = \ln(q_e) - k_1 t \tag{38}$$

where $q_t$ and $q_e$ (for each species) are the amounts of metal ions adsorbed at time $t$ and equilibrium in mg/g, respectively, $t$ is the time in min and $k_1$ the rate constant of the equation in $\text{min}^{-1}$. The biosorption rate constants ($k_1$) can be determined by plotting ln ($q_e - q_t$) versus $t$. The pseudo-second-order model predicts the behavior over the complete adsorption period and is in agreement with the adsorption mechanism being the rate-controlling step. This model is shown below, as in Equation (38):

$$q_t = \frac{k_2 {q_e}^2 t}{1 + K_2 q_e t} \tag{39}$$

This equation can be rearranged in linear form, as in Equation (39):

$$\frac{t}{q_t} = \frac{1}{k_2 {q_e}^2} + \frac{t}{q_e} \tag{40}$$

$q_e$ is the maximum removal rate for a specific cation (in a multicomponent phase) when equilibrium is achieved. The applicability of the pseudo-first-order (Equation (22)) and pseudo-second-order kinetic models (Equation (25)) has been used to validate experimental data where $k_2$ is the rate constant of the second-order equation in g $\text{mg}^{-1}$ $\text{min}^{-1}$, $q_t$ is the biosorption capacity at time $t$ in mg/g and $q_e$ is the biosorption capacity at equilibrium in mg/g [89]. However, it must be assessed whether the presence of several functional groups in a bioadsorbent requires kinetic rate constants ($k_1$ and $k_2$) to be treated as a lumped coefficient. Thus, the pseudo-first- and second-order models are inadequate to precisely quantify adsorption behavior.

2.2.2. External Mass Transfer Model

The external mass transfer is represented by Equation (41) [100]:

$$\left[\frac{d(C_t/C_i)}{dt}\right]_{t=0} = -k_{ES} \tag{41}$$

where $C_i$ and $C_t$ (mmol/L) are the contaminant concentrations in an aqueous phase at time intervals $t$-0 and $t$-$t$, respectively

The authors state that Equations (40) and (41) assist in analyzing the role of intraparticle diffusion and external mass transfer processes, respectively. However, a limitation is observed in that they fail to attribute the impact of the models with respect to the dominance of either intraparticle or external mass transfer processes. The Boyd's plot is obtained by plotting $B.t$ versus time $t$. The value of $B.t$ can be calculated from Equation (42) [101]:

$$B.t = -0.4977 - \ln\left(1 - \frac{q_i}{q_\infty}\right) \tag{42}$$

where $q_t$ and $q_\infty$ are the amounts of metal adsorbed (mmol/g) at time t and infinite time, respectively. External mass transfer is the dominant rate process if the Boyd's plot displays linearity and does not pass through the origin. $B$ is a parameter ($\text{h}^{-1}$.) and is a function of the ratio of diffusivity to the square of the radius of the adsorbent.

**Table 4.** Equilibrium isotherms and reaction kinetics models.

| Model | Type | Formula |
|---|---|---|
| Langmuir [90] | Isotherm model | $\frac{Q}{Q_{max}} = \frac{LC}{1+LC}$ |
| Langmuir with competition between two species $i$ and $j$ [91] | Isotherm model | $Q_i = Q_{max,i}\frac{L_iC_i}{1+L_iC_i+L_jC_j}$ |
| Langmuir with competition between q species [92] | Isotherm model | $Q_i = Q_{max,i}\frac{L_iC_i}{1+\sum_{j=1}^{q} L_jC_j}$ |
| *Langmuir–Freundlich* [90] | Isotherm model | $\frac{Q}{Q_{max}} = \frac{LC^n}{1+LC^n}$ |
| Generalized Langmuir [93] | Isotherm model | $\frac{Q}{Q_{max}} = \left(\frac{LC}{1+LC}\right)^n$ |
| Redlich–Peterson [94] | Isotherm model | $\frac{Q}{Q_{max}} = \frac{LC}{1+(LC)^n}$ |
| Toth [95] | Isotherm model | $\frac{Q}{Q_{max}} = \frac{LC}{\left[1+(LC)^n\right]^{\frac{1}{n}}}$ |
| Hinz [96] | Isotherm model | $Q = Q_{max}\sum_{i=1}^{\omega} f_i \prod_{j=1}^{\tau_i}\left(\frac{A_{i,j}C^{p_{i,j}}}{1+B_{i,j}C^{q_{i,j}}}\right)^{r_{i,j}}$ |
| First order [97] | Kinetic model | $\frac{dQ}{dt} = \frac{\theta}{\rho}k_1C - k_{-1}Q$ |
| nth order [97] | Kinetic model | $\frac{dQ}{dt} = \frac{\theta}{\rho}k_1C^n - k_{-1}Q$ |
| Langmuir kinetic [97] | Kinetic model | $\frac{dQ}{dt} = \frac{\theta}{\rho}k_1C(Q_{max} - Q) - k_{-1}Q$ |
| Langmuir kinetic with competition between n species [98] | Kinetic model | $\frac{dQ}{dt} = \frac{\theta}{\rho}k_{1,i}C_i\left(Q_{max} - \sum_{j=1}^{n} Q_j\right) - k_{-1,i}Q_i$ |
| First order with partly pseudo-irreversible adsorption [99] | Kinetic model | $\frac{dQ}{dt} = \frac{\theta}{\rho}k(C - C_{irr})$ |

A well-known approximation model for intraparticle diffusion is explained by the modified equation below [101]:

$$B.t = -\ln\left[1 - \left(\frac{q_t}{q_e}\right)^2\right] \quad (43)$$

In this above equation, the plot displays a straight line passing through the origin. Further, a film-based diffusion control mechanism coupled with a Langmuir isotherm model assists in developing a kinetic model that aids in quantifying the mass transfer rate as [101]:

$$\frac{dq_t}{dt} = \frac{3K_f}{R\rho_P}(C_b - C_s) \quad (44)$$

2.2.3. Multicomponent Surface Excess Kinetic Model

A simulation model based on the surface excess concept can be developed, and the output simulated data may display excellent agreement with the experimental results [102].

Often, the adsorption of cations in a bioadsorbent is summarized as a two-step reaction mechanism. The rate-limiting step (second step) is preceded by a fast step that reveals that resistance to mass transfer in the double layer (encapsulating the substrate) is negligible. It has been observed that, initially, the number of active sites available for adsorption is significantly high. Hence, if the surface coverage of the contaminant on the substrate is insignificant, the reaction rate is high. However, with an increase of surface coverage, the rate of the reaction decreases, as few interaction sites remain available for adsorption. Thus, the difference between the actual amount of cation in the bulk phase and the amount of cation that would be present in the adsorbed phase is defined on the basis of the surface excess concept [103]. Equations (33) and (34) are based on the surface excess concept, and the kinetic model is evaluated using simple first-order kinetics [104]:

$$\frac{\partial {n_1}^{ea}}{\partial t} = K_1({n_1}^{e} - {n_1}^{ea}) \tag{45}$$

where ${n_1}^{e}$ is the equilibrium surface excess (of cation 1) given by (kg of solute 1 per unit kg of solid) and ${n_1}^{ea}$ is the actual surface excess (of cation 1) provided by kg of solute 1 per unit kg of solid:

$${n_1}^{ea} = \left( \frac{m_1 x_1 S}{S x_1 + \frac{m_1}{m_2}} \right) x_2 \tag{46}$$

$k_1$ is an adsorption constant when ${n_1}^{e} > {n_1}^{ea}$;
$m_1$ is monolayer coverage of component 1 (solute) per unit mass of the adsorbent, (kg/kg);
$m_2$ is monolayer coverage of component 2 (solvent) per unit mass of the adsorbent (kg/kg);
$x_1$ is the mass fraction of the solute in the bulk phase;
$S$ is the selectivity factor, a dimensionless parameter (maximum value of unity).

Overall, it is elucidated that the sorption kinetics of a reaction are dependent on both the concentration of the ions in the bulk and adsorbed phases and on the availability of binding sites in the substrate.

#### 2.2.4. Pore Diffusion Model

The pore or intraparticle diffusion model proposed by Weber and Morris is employed for the diffusion mechanism, described as [105]:

$$q_t = k_i t^{1/2} + \frac{1}{C} \tag{47}$$

where $k_i$ is the intra-particle diffusion rate constant in mg $g^{-1}$ $min^{-0.5}$ and $C$ is the constant that provides intraparticle accumulation in the boundary layer in mg/g.

The mechanism that couples pore diffusivity followed by the chemisorption of ions is displayed via the hybrid model of Equation (32) [105]:

$$q_t = k_i t^{1/2} + \frac{1}{\frac{1}{k_2 {q_e}^2} + \frac{t}{q_e}} \tag{48}$$

In correlation to the biosorption of Ni(II) ions on sludge waste, a pseudo-second-order kinetic model ($R^2 \approx 0.99$) fits the experimental data. This indicates that the surface reaction that bears the ion exchange mechanism is the rate-controlling step for the biosorption of Ni(II) and Cd(II) ions by the sludge [106].

The concentration gradient between the bulk and adsorbed phases provides the driving force in overcoming the mass transfer resistance to adsorption of Ni(II) ions [107]. The researchers have observed that the percent of Ni(II) removal is inversely proportional to the initial metal ion concentrations. The metal uptake decreases as its concentration of adsorbed ions increases. However, the amount of Ni(II) ions adsorbed per unit mass of the biosorbent increases with an increase in the initial ion concentrations.

However, multicomponent adsorption demands that a concentration of specific ionic species and their corresponding competitive kinetic interactions with specific functional groups (interaction sites) will aid in determining the rate of removal of ions from the bulk phase to the adsorbed phase. Hence, several models have been discussed in the manuscript that incorporate the number of available free interaction sides and a combined surface and pore diffusion formulation to validate experimental data with simulated runs.

However, because the kinetic parameter, $k_1$, is a lumped coefficient, and the effect of internal porosity (with respect to biosorbents) is a dominant parameter, the assumption holds valid that intraparticle diffusion is dependent on pore volume diffusion, and the adsorption rates (following pore diffusion) in active sites are instantaneous [64].

The pore diffusion-based rate equation quantifies the mass balance of contaminant A exiting the bulk phase into the adsorbed phase. The researchers performed the mass balance for contaminant A as follows:

$$\varepsilon_p \frac{\partial C_{A,r}}{\partial t} + \rho_b \frac{\partial q}{\partial t} = \frac{1}{r^2}\frac{\partial}{\partial r}\left[r^2\left(D_{e,p}\frac{\partial C_{A,r}}{\partial r}\right)\right] \quad (49)$$

where

$D_{e,p}$—effective diffusivity;
$\varepsilon_p$—bed porosity;
$r$—distance of spherical particle from center of sphere;
$\rho_b$—Bed density;
$R$—radius of sphere;
$C_A$—Concentration of species A;
Boundary condition 1: At $r = 0 \rightarrow \frac{\partial q}{\partial r} = 0$;
Boundary condition 2: At $r = R \rightarrow \rho D_s\left(\frac{\partial q}{\partial r}\right)_{r=R} = K_f a(C - C_s)$;

and where

$D_s$—surface diffusivity;
$K_f$—film diffusion coefficient;
$a$—surface area of the pellet.

Thus, the combined pore and surface diffusion model can be represented as [71]:

$$\varepsilon p\frac{\partial C_A}{\partial t} + \rho\frac{\partial q_A}{\partial t} = \frac{D_{s\,A}}{r^2}\frac{\partial}{\partial r}\left(r^2\frac{\partial q_A}{\partial r}\right) + \frac{\rho D_{ep\,A}}{r^2}\frac{\partial}{\partial r}\left(r^2\frac{\partial q_A}{\partial r}\right) \quad (50)$$

The boundary conditions are:

$$\begin{gathered} At\ r = 0 \rightarrow \frac{\partial q}{\partial r} = 0 \\ At\ r = R \rightarrow \left[\left(D_{ep_A} + D_{s_A}\rho\frac{dq}{dC}\right)\frac{\partial C}{\partial r}\right]_{r=R} = k_f(C_A - C_{s\,A}) \end{gathered} \quad (51)$$

If $\rho\frac{\partial q_A}{\partial t} \gg \frac{\partial C_A}{\partial t}$, the diffusion equation can be expressed as

$$\frac{\partial q_A}{\partial t} = \frac{1}{r^2}\frac{\partial}{\partial r}\left(D_{ep\,A}r^2\frac{\partial q_A}{\partial r}\right) \quad (52)$$

When additional reaction occurs in the bio adsorption process

$$\frac{\partial q_A}{\partial t} = \frac{1}{r^2}\frac{\partial}{\partial r}\left(D_{ep_A}r^2\frac{\partial q_A}{\partial r}\right) + R_A \quad (53)$$

where

$$R_A = K_A(q_{A_e} - q_A) \quad (54)$$

$K_A$ is the overall kinetic constant of A (in a multicomponent phase) with respect to several functional groups in the adsorbent.

In relation to distinct rate-controlling steps, the appropriate rate-controlling mechanisms should incorporate film pore diffusion, film surface diffusion and film pore–surface-diffusion models. In general, film diffusion behavior is limited and is associated with a negligible concentration gradient [70]. Further, a close preview of Equations (35)–(39) indicates that the rate of surface diffusion mechanism is significant and is seldom applied as a rate-controlling step.

(i) Macro pore diffusion

Depending on the relative magnitude of pore diameter in the adsorbent molecule, transport through a macropore can occur via several mechanisms [108]. Thus, if the packed bed is composed of adsorbent particles of varying pore sizes, the pore diffusivity can be characterized by further classification of pore diffusion.

(ii) Micro pore diffusion

The defined branched pore model kinetics are based on the assumption that each adsorbent pellet is composed of micropores (radial size < $r_c$) and macropores (radial size ($r_c < r_p$)), where $r_p$ is the radial distance from the center of the pore to the outer boundary

affected by surface diffusion and $r_c$ is the radial distance from the center of the pore to the inner boundary of the surface diffusion. The underlying feature of reaction kinetics is that chemisorption is preceded by both surface and pore diffusion, and the overall diffusion mechanism can occur either simultaneously or in a sequential order with surface diffusion in the initial step.

## 3. Fixed-Bed Dynamic Model

### *3.1. Uni Component Model*

Single-component metal ion adsorption behavior, with respect to breakthrough characteristics, is directly proportional to variations in bed height and pH levels in the bulk phase. Conversely, breakthrough intervals decrease with an increase in flowrates and concentrations of metal ions in the bulk phase [109]. In addition, with respect to a heterogeneous substrate, the two kinetic site models, with respect to a biomass, such as moss, are associated with sorption by a rate-limited reaction. A two-site model with specific activity coefficients is incorporated into the equation.

Suzaki et al. studied the dynamics of adsorption of monocomponent heavy metal ions (Cu(II), Ni(II) and Zn(II)) in a fixed-bed column with the residue of an extraction from Sargassum pendula, a type of seaweed. They used a phenomenological mathematical modeling technique to describe the dynamics and to propose a rate-limiting step. Figure 2A shows a schematic of a fixed-bed column fed with concentration C_jˆf, which enters the column and leaves at a concentration of C_jˆout. Mass balance was carried out in a finite section of the column. Internal mass transfer, external mass transfer and adsorption of the metal on the active sites were incorporated into the model. Langmuir isotherm was used to model the equilibrium data for each metal ion in the bioadsorbent. Figure 2B–D show that the Langmuir isotherms accurately fit the equilibrium data. Figure 2D shows the curves of experimental data and the model-predicted breakthrough curves for the different ions at different inlet concentrations. The model-predicted curves were generated using internal mass transfer resistance (IMTR), external mass transfer resistance (EMTR) and the adsorption of metal ions in the active sites (ASA) as rate-limiting steps. It can be inferred from the curves that the curve predicted using the IMTR as a rate-limiting step fitted the experimental results more closed compared to the models using EMTR and ASA as rate-limiting steps [110].

Several dynamic models are displayed in Table 5 that partially address the breakthrough behavior in the fixed-bed dynamic column.

Rahman et al. [116] modeled the bioadsorption of arsenic ions in fish scales using the surface excess model with a 2D transport model. Figure 3A–D demonstrates the experimental results as well as the corresponding simulation profiles of Runs 1–4. These runs were conducted with cod scales with a fixed-bed flow column to remove As (III) ions at different operating conditions of concentration and flowrate. Figure 3A represents the breakthrough curves for Run 1. The break point was observed at 7 h, and the column was fully exhausted after 20 h of operation. It was observed that the relative effluent concentration remained below 0.1 for the first 7 h. After this, the outlet concentration increased sharply, and eventually, adsorption significantly decreased after 20 h. The numerical results suggest that the experimental breakthrough occurs earlier.

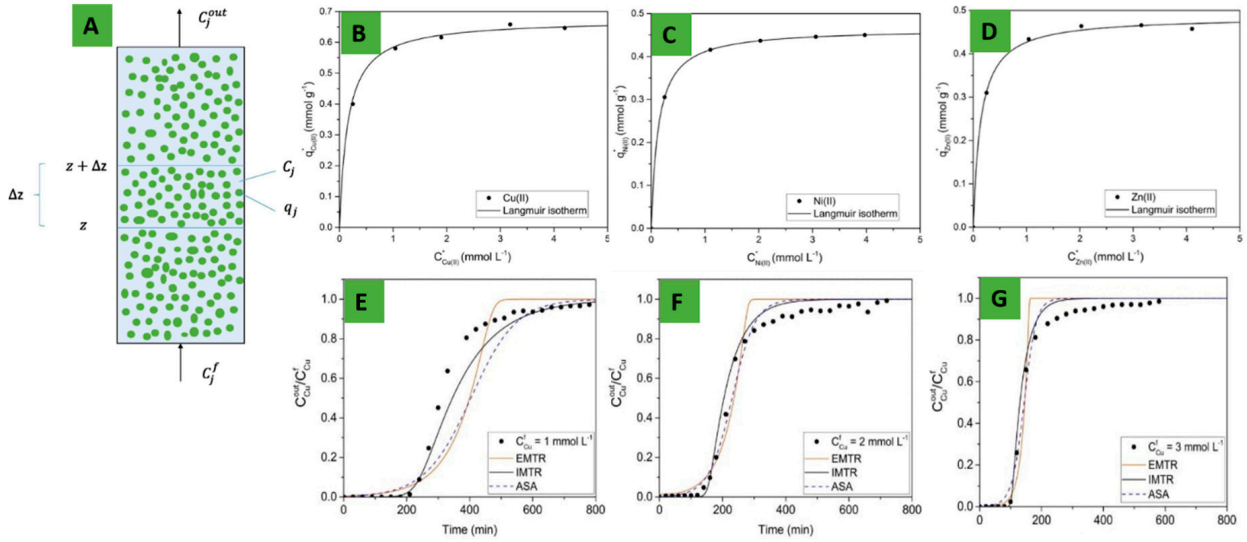


**Figure 2.** (**A**) A schematic of the adsorption of metal in a fixed-bed column. Experimental equilibrium isotherms fitted according to the Langmuir model for monocomponent adsorption in a fixed-bed column of ions Cu(II) (**B**), Ni(II) (**C**) and Zn(II) (**D**). Experimental conditions: initial pH of 4.0, average particle diameter of 0.61 mm, flow of 3 mLmin$^{-1}$ bed length of 12 cm, 2 g of biomass, bed porosity of 0.28 and temperature of 25 °C. (**E**–**G**) Experimental and modeled breakthrough curves for monocomponent adsorption in the fixed column of the Cu ion with initial concentrations of 1, 2 and 3 mmol L$^{-1}$. Experimental conditions: initial pH of 4.0, average particle diameter of 0.61 mm, flow of 3 mLmin$^{-1}$, bed length of 12 cm, 2 g of biomass, bed porosity of 0.28 and temperature of 25 °C, adapted with permission from Ref. [110]. 2017, Elsevier.

**Table 5.** A brief summary of the various models applicable to correlation of dynamic column biosorption data.

| MODELS | Equation | Parameters Involved |
|---|---|---|
| Linearized Thomas model [111] | $\ln\left(\frac{C_0}{C_i}-1\right)=\frac{K_{Th}q_0m}{Q}-K_{Th}C_0t$ | $K_{Th}$: Adsorption constant<br>$q_0$: Adsorption capacity<br>$m$: mass of adsorbent |
| Adams–Bohart model [112] | $\ln\left(\frac{C_t}{C_0}\right)=K_{AB}C_0t-K_{AB}N_0\frac{z}{U_0}$ | $K_{AB}$: reaction rate constant (mL/mg.min)<br>$N_0$: solubility (mg/L)<br>$z$: bed height (cm)<br>$U_0$: flowrate (cm/min)<br>$Q_v$: flowrate (L min$^{-1}$) |
| Yoon–Nelson model [113] | $q_B = Q_v(C_o - C_b/2)t_B/m_{adsorbent}$ | $C_o$: influent metal ion concentration<br>$C_b$: breakthrough metal ion concentration<br>$q_B$ breakthrough adsorption capacity (mg/g) |
| Carman equation [114] | $\Delta P_{pb}=F_w\frac{f_a(1-\varepsilon)h\rho\frac{Q_1{}^2}{A_1{}^2}}{g\varepsilon^3}$<br>$R_{e_p}=\frac{vd_p}{\mu}$ | $a$ : mass specific transfer area (cm$^{-1}$)<br>$R_{e_p}$: Reynold's number of particle<br>$\Delta P_{pb}$: packed bed pressure drop (Pa)<br>$F_w$: wall effect factor (−/−)<br>$f$: friction parameter<br>$Q_1$: flowrate (L min$^{-1}$)<br>$A_1$: outlet cross-sectional area<br>$h$: bed height (cm)<br>$\varepsilon$: porosity of bed<br>$\mu$: kinematic viscosity (cm$^2$/min) |
| Fate contaminant model [115] | $\left(1+\frac{\rho_b}{\varepsilon_b}\frac{bc}{(1+bc)^2}\right)\frac{\partial C}{\partial t}=D\frac{\partial^2C}{\partial x^2}-u\frac{\partial C}{\partial x}$ | C—ion concentration in the column void;<br>$u$—pore velocity, cm s$^{-1}$;<br>$D$—axial dispersion, cm s$^{-2}$;<br>$\rho_b$—bulk density, g cm$^{-3}$. |

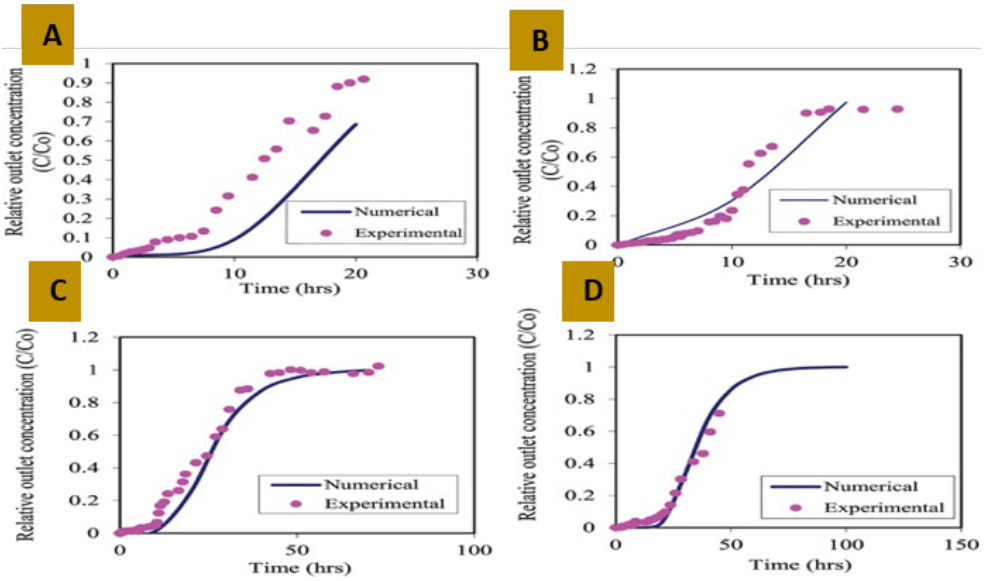


**Figure 3.** Comparison of experimental and numerical results of As(III) removal in codfish scale-packed columns: (**A**) Run 1: Mass of adsorbent = 61.54 g of dried cod scales, concentration of arsenic (III) solution = 41,220 mg/L, pH = 8.7 and flowrate to the column = 2 mL/min. (**B**) Run 2: Mass of adsorbent = 66.87 g of dried cod scales, concentration of arsenic (III) solution = 82,760 mg/L, pH = 9.25 and flowrate to the column = 2.75 mL/min. (**C**). Mass of adsorbent = 66.87 g of dried cod scales, concentration of arsenic (III) solution = 41,220 mg/L, pH = 9.25 and flowrate to the column = 2.75 mL/min. (**D**) Run 4: Mass of adsorbent = 69.544 g of dried cod scales, concentration of arsenic (III) solution = 520 mg/L, pH = 8.7 and flowrate to the column = 2 mL/min, adapted with permission from Ref. [116]. 2015, John Wiley and Sons.

Limitations of the Abovementioned Models

With respect to the models introduced in Table 5, it has been reported that the adsorption capacity of a metal ion is enhanced by increasing the pore size of an adsorbent [87]. However, after reviewing the above models, it can be concluded that the concept of internal porosity in an adsorbent has been ignored in the quantification process. The concept of porosity in correlation to adsorption mechanisms is a DUAL POROSITY concept that incorporates external voidage and internal porosity [25]. The researchers propose a three-way partition of the porous medium that includes (a) a solid phase, (b) a pore phase and (c) a bulk phase. At lower internal porosity conditions, the pore diffusivity of a cation (with respect to a larger atomic weight, such as in lead ions) is significantly limited. Conversely, a reduced external voidage in an adsorbent invokes a tortuous path for the effluent (in the bulk phase), which results in an increase in the adjective forces of the ion and, simultaneously, a decrease in the breakthrough time intervals. However, simultaneously, it can be concluded that a diffused ion in a mitigated pore diameter is highly susceptible to attenuation at its substrate due to a reduced distance between the interactive forces. The ratio of internal porosity to external voidage is directly proportional to the absorptivity of that ion. In addition, it must be validated that the mobility of an ion and the pH of the bulk phase significantly contribute to the adsorption of the ion. The mobility of an ion is directly proportional to the flowrate of the effluent phase and inversely correlated to the atomic size of the contaminant ion. The ratio between the atomic weight of the ion and the molecular weight of water is equivalent to the retardation factor of the ion, and a decrease in the retardation factor is proportionally linked to the abatement of absorptivity in an ion. However, the models displayed in Table 5 have not quantified these effects comprehensively. These models have failed to emphasize the variation in the absorptivity of a specific ion in the presence of several contaminant ions. The pH sensitivity to adsorption must include the hydronium ion as an interfering ion in a bulk phase. Further, it has been documented that, at higher flow rates, an increase in the pH condition of a bulk phase results in early

breakthrough intervals with respect to the contaminant. This phenomenon is compounded by the fact that, at both higher pH and effluent flowrates, the dominance of adjective forces prevail over electrostatic forces between the ion and the substrate.

The adsorption of specific ions in a multicomponent phase is affected by the intrinsic sorption coefficients, the pH of the bulk phase and adsorbent characteristics, which includes the flowrate of the effluent. The concept of the retardation factor (as a function of inverse mobility) is that, the higher the atomic weight of an ion, its retardation (in a porous medium) is proportionately higher. In other words, lead ions with a larger atomic weight display lesser mobility (or a higher retardation factor) compared to sodium ions with a correspondingly lower atomic weight in a porous adsorbent. The higher the mobility of an ion, the more its adsorption behavior, in terms of breakthrough time, decreases. In short, contrary to expectations [21], with an increase in both the pH and flowrate, the break through interval, after a certain level, decreases. The adsorption mechanism is a competition between electrostatic forces in association with the specific ion and the specific site of the adsorbent. The mobility of the specific ion in the pore phase of the adsorbent is inversely proportional to its retardation factor. Overall, it can be elucidated that, at a specific range of conditions, the adjectival forces will prevail over electrostatic forces of attraction, leading to early breakthrough behavior. At creeping velocities (extremely low Reynold's numbers), the breakthrough behavior increases with the flowrate. However, after a specific range of flowrates (where a constant value of breakthrough interval is observed), the breakthrough interval decreases with a proportional increase in flowrates [117]. Experimental data confirms that adsorption capacity increases with an increasing inlet concentration and bed depth and, conversely, decreases with an increasing flowrate. The Thomas, Yoon–Nelson and Adams–Bohart models were used to analyze the column experimental data and monitor the sensitivity of the operating parameters [113].

In dynamic adsorption processes, the effluent flows continuously through a column of the adsorbent or a packed bed, where an ion from the bulk phase is transferred to the solid phase. The adsorptive performance of an adsorbent is a consequence of capacity and kinetics. The conventional approach to evaluating this performance is based on a two-step procedure [116]: (1) the generation of equilibrium isotherms and (2) the operation of pilot columns. An isotherm indicates the capacity of an adsorbent for removing solutes from water and wastewater.

Fixed-bed kinetic sorption (Adams–Bohart, Thomas, Yoon–Nelson, Clark, Wolborska, and modified dose-response) models are commonly used to simulate breakthrough curves (BTCs) in fixed-bed systems [112]. However, the major deficiencies with these models are that they are not sufficient to comprehensively define the specific interaction between a specific ion and a specific functional group in the substrate. In addition, the models mentioned above fail to address the concept of surface diffusion coupled with the porosity of a mesoporous bioadsorbent. Hence, it is imperative to study surface excess and pore diffusion models that adequately validate the biosorption process [21,25,106,116]. The significance of these models is that they include ionic diffusion as a rate-controlling step, which precedes the chemisorption of the contaminant ion with the biomass.

In brief, it is essential to observe the overall concept of multicomponent adsorption as a function of several factors in correlation to each component in the presence of several interfering ions and the pH of a medium. The adsorption of an ion is highly sensitive to the pH of the bulk phase because the strength of hydronium ions, coupled with the speciation of the contaminant (at specific pH conditions), significantly contributes to the sorption behavior of specific species in both batch and dynamic column runs.

### *3.2. Multicomponent Dynamic Models*

The concentration profile of the exit stream from the dynamic adsorption column is plotted as a function of the time interval. The evaluation of the breakthrough time interval and the steady state concentration of the exit stream is indispensable for the appropriate design of a fixed-bed adsorption column [117]. The significance of parameters such as

flowrate, the inlet concentration of the influent and the bed height of the adsorbent column bear a profound effect on the breakthrough characteristics of a dynamic column run [118].

The Thomas model is one of the most widely used models in describing column performance and predicting BTCs. It assumes a plug flow behavior in the bed, and the rate-driving force in adsorption follows both the second-order reversible kinetics reaction and the Langmuir isotherm model [119]. The model can be represented by the equation below:

$$\frac{C_t}{C_0} = \frac{1}{1 + \exp\left[\left(\frac{K_T}{Q}\right)(q_0 m - C_0 Q t)\right]} \tag{55}$$

In addition, the BDST model displays the linear correlation between the bed depth of the column and service time with adsorption parameters and process concentration. The assumption of this model is that the external mass transfer resistance and intraparticle diffusion type forces are negligible. Thus, the surface chemisorption of the unused adsorbent and the solute in the liquid phase can control the adsorption kinetics. The model provides a comparison between the adsorption capacities of the columns operated under various process conditions [120]:

$$t = \left(\frac{N_0 H_t}{C_i U}\right) - \left(\frac{1}{K_0 C_i}\right) \ln\left(\frac{C_i}{C_t} - 1\right) \tag{56}$$

However, the mass transfer coefficients and effective diffusivities determined from the experimental adsorption data have demonstrated that the parameters bear a dominant effect on the adsorption mechanism [121].

Therefore, the assumption that the overall sorption rate is controlled solely by heavy metal diffusion is reasonably logical, and the Langmuir isotherm model is applicable for ion exchange rate calculations for a biosorbent over a wide concentration range [122]. However, very few citations have revealed the significance of dynamic column biosorption studies with respect to multicomponent species.

The governing equations are as follows:

#### 3.2.1. Entrapment Model

With respect to multicomponent adsorption, a single dimensional mass transfer equation that includes mechanical entrapment in the adsorbent is provided as [123]:

$$\frac{\lambda q \rho_1}{A\phi}\frac{\partial^2 x_1}{\partial x^2} - \frac{q\rho_1}{A\phi}\frac{\partial x_1}{\partial x} = \frac{1-\phi}{\phi}\rho_r\left[n_0\frac{\partial x_1}{\partial t} + \frac{\partial {n_1}^{ea}}{\partial t} + V\right] \tag{57}$$

Further, the researchers have concluded that the central concept behind the theory of mechanical entrapment term is the representation of both particle and pore size distributions by partitioning the porous medium at any cross-section into pluggable and non-pluggable pathways.

The total deposition is related to the depositions of pluggable and non-pluggable pores and is defined as:

$$\phi_i V = fV_p + (1-f)V_{np} \tag{58}$$

However, in porous media with relatively high porosities, such as fish scales (a biosorbent), entrapment due to pluggable pores is negligible. Thus, the value of $f$ in Equation (38) is reduced to zero [25].

#### 3.2.2. Two-Dimensional Dispersion Model

Based on the mesoporous characteristics of a biosorbent, a 2D advection–dispersion equation must include the surface excess variables coupled with both Darcy's law and the diffusivity equation. These are solved simultaneously and discretized using the finite difference technique. The governing equations can be expressed as follows [115]:

$$Dx\rho_l\frac{\partial^2 x_1}{\partial x^2} + Dy\rho_l\frac{\partial^2 x_1}{\partial y^2} - \omega\frac{u\rho_l}{\phi}\frac{\partial x_1}{\partial x} - \omega\frac{v\rho_l}{\phi}\frac{\partial x_1}{\partial y} = \frac{1-\phi}{\phi}\rho_a {n^0}\frac{\partial x_1}{\partial t} + \frac{1-\phi}{\phi}\rho_a {n^0}\frac{\partial {n_1}^{ea}}{\partial t} \tag{59}$$

The Darcian velocity with respect to the $x$ and $y$ directions can be expressed as:

$$u = -\frac{\alpha_c \beta_c k}{\mu} \frac{\partial P}{\partial x} \tag{60}$$

$$v = -\frac{\alpha_c \beta_c k}{\mu} \left( \frac{\partial P}{\partial y} - \gamma_c \rho g \right) \tag{61}$$

By coupling Equations (45), (60) and (61) into Equation (59), the diffusivity equation can be formulated as:

$$\frac{\phi \mu c}{\alpha_c \beta_c k} \frac{\partial P}{\partial t} = Dx\rho_l \frac{\partial^2 P_1}{\partial x^2} + Dy\rho_l \frac{\partial^2 P_1}{\partial y^2} \tag{62}$$

The pressure drop across a packed bed can be represented with the Ergun model, as [124]:

$$\frac{\Delta P}{\Delta L} = \frac{150 \mu U_0}{{d_P}^2} \frac{(1-\varepsilon)^2}{\varepsilon^3} + \frac{1.75 \rho_f (U_0)^2}{d_P} \frac{(1-\varepsilon)}{\varepsilon^3} \tag{63}$$

Since the fluidized bed pressure drop is equal to the effective weight of the solid in the bed, the pressure drop can be expressed as:

$$\frac{\Delta P}{\Delta L} = \left( \rho_b - \rho_f \right) g = (1-\varepsilon) \left( \rho_P - \rho_f \right) g \tag{64}$$

The bulk density of the bed and the average diameter of the solid adsorbent can be represented by:

$$\rho_b = (1-\varepsilon)\rho_P + \varepsilon \rho_f \tag{65}$$

$$\frac{1}{D_{av}} = \frac{X_1}{D_1} + \frac{X_2}{D_2} \tag{66}$$

The Darcian velocities of Equations (60) and (61) can be determined by coupling Equation (63) with Equations (64)–(66).

#### 3.2.3. Pore Diffusion Model

The disadvantage of the surface excess model is a lack of sensitivity to the quantification of absorptivity with respect to the distribution of adsorption sites within the internal walls of a pore [21]. In the "pore diffusion model", diffusion is assumed to occur in the fluid phase with a distributed adsorption along pore walls. There is a three-way division of bed volume (internal porosity, external voidage and solid mass), and contaminant diffusion occurs in an internal void fraction [50]. The "porosity" parameter is accommodated by the concept of both pore and surface diffusion. In addition, access to pore diffusion limits the overall rate of adsorption, and the value of the overall pore diffusion coefficient is inversely proportional to the pressure applied on an effluent solution in correlation to dynamic column adsorption [125,126].

Each specific component's interaction between the respective bulk and adsorbed phases can be validated by the pore diffusion mechanism. In relation to bioadsorbents, the considered assumptions are that particles are spherical in shape and are homogeneous in size. Each spherical particle has a well-defined pore in which contaminants diffuse and are adsorbed on the internal walls of the pore [21]. Further, the researchers have concluded that the abatement of contaminants in the substrate of a sphere may be assumed to be negligible, and a constant contaminant concentration (xs) of a thin fluid film is invoked at the outer boundary of the adsorbent. This film, which encapsulates each particle due to the saturation of the medium with deionized water before the addition of the contaminant solution, acts as resistance to the mass transfer of solute between the bulk phase and the surface of the adsorbent.

The mathematical model is initiated with the following assumptions [127]:

(i) Equilibrium occurs between the pore liquid and particle interior; i.e., the solution flow to the pores is much faster than its uptake at sorption sites.

(ii) Mass transfer in the pores is solely based on molecular diffusion; i.e., it follows Fick's first law and is measured by the effective pore diffusion coefficient, $D_{eff}$.

(iii) Solute concentration in the pore liquid is very small relative to that in the adsorbed phase and can therefore be neglected.

The pore diffusion model is extremely sensitive to the ratio of internal porosity to external voidage. Hence, it is imperative to elucidate the partition of flow with respect to pore and surface diffusivities before incorporating the velocity vector and retardation factor of the solute in the overall effluent concentration rate equation.

After the partition of flow in the external voidage and internal porosity, if the molar flowrate of a specific ion is $V$, a concentration profile with respect to voids ($y$), concentrations at pore phases ($x$), time intervals ($t$) and the heights of the column ($z$) can be determined. Both the initial and boundary conditions can be incorporated into equations in Equations (67) and (68), respectively [21].

$$\text{At time } t = 0,\ y = 0 \tag{67}$$

($y$ is the mole fraction of the solute in pore phase)

$$\text{At } Z = 0,\ V_{p1} + V_{v1} = V \text{ for } t > 0 \tag{68}$$

If $V$ moles of an ion are moving through a column per unit time,

$$V_{p1} = x\ (V_p, \text{ total molar flowrate through pores}) \tag{69}$$

$$(V_v, \text{ total molar flowrate through the voids}) \tag{70}$$

$$\frac{V_p}{V_v} = \left(\frac{\alpha}{\varepsilon}\right) \tag{71}$$

where $V_{p1}$ and $V_{v1}$ are moles of ion concentrations at the pore and void spaces, respectively, of the inlet of the column. It must be noted that the effluent is injected in the bioadsorbent column against gravity. The researchers have concluded that the ratio of molar flow through external voidage and internal porosity is directly correlated to the ratio of external voidage and internal porosity.

In order to characterize transport through a dynamic column, the model coupled the velocity factor with the mass balance equation, which is expressed as:

$$v\frac{\partial y_i}{\partial z} + \frac{\partial y_i}{\partial t} = -\frac{A}{\rho\varepsilon}\left(\frac{\alpha}{1-\varepsilon}\right)k_{fi}(y_i - x_{si}) \tag{72}$$

Further, a series of partial differential equations aids in the quantification of contaminant transport through a porous medium by considering both the dispersion and retardation coefficients of several competing ions in an effluent [21].

In addition, the model assessed that dynamic equilibrium is when ions in the adsorbed phase bear a direct correlation to the ions in the pore phase. This adsorbed phase includes the sites already occupied by the sorbate at earlier time intervals. In other words, when the sites become saturated with ions, further immobilization of ions on the internal walls of the substrate is terminated.

Differentiating Equation (30) with respect to x and coupling Equations (67) and (72) into the expression, a mass-transfer balance is attained as:

$$\begin{aligned} v\left(\tfrac{\partial y}{\partial z}\right) + \tfrac{\partial y}{\partial t} = \ & -\left(\tfrac{A}{\rho\varepsilon}\right)\left(\tfrac{\alpha}{1-\varepsilon}\right) \\ & \left[D_p\tfrac{\rho}{1-x} + \rho_a\tfrac{D_s}{\alpha}\left[\left(\tfrac{1-\varepsilon}{\rho_a}\right)(Q_m d - 1)\left[\rho(1+d\rho x) - d\rho^2 x\right] \times \left(\tfrac{1}{1+d\rho x}\right)^2\right]\right] \end{aligned} \tag{73}$$

Equation (73) quantifies the concentration fluctuations with respect to time intervals at specific heights of the column. The researchers propose an explicit time–center space forward scheme to compile the numerical code. Nested DO loops, with respect to discrete time and space intervals, can be utilized for simulated models. The code permits the

utilization of partial differential equation to solve for other concentration values in future time steps.

## 4. Overall Review of the Batch and Dynamic Models

The following procedures, in ascending order, are the ultimate route to improved methods for analyses of complex physical and chemical phenomena:

(i) Mathematical models.
(ii) Bench scale experimental models
(iii) Numerical and experimental (unscaled) procedures.
(iv) Scaled experimental models (prototypes).
(v) Experimental, scaled and numerical models [42].

In short, in order to develop numerical models that can validate scaled-up experimental data in a process where dynamic equilibrium and gravitational forces are significant factors, the elucidation of the process in association with its reaction kinetics is extremely indispensable. A chemical process, such as adsorption, will require a comprehensive review of the dispersion and retardation mechanisms. Under such conditions, various models were considered for appraisal. Given the mesoporous nature of a biomass, such as fish scales, the pore diffusion multicomponent model in both batch and dynamic states is highly applicable.

Most biomasses are heterogeneous in nature (inheriting several functional groups as interaction sites). The surface characterization of fish scales has revealed that interaction sites are oriented toward the internal walls of the pores. Hence, the value of internal porosity is important to quantify the adsorption process. Thus, the scope of the surface excess and entrapment models is limited with respect to pH fluctuations and competitive sorption mechanisms

## 5. Conclusions and Recommendations

The mathematical modeling of the biosorption process is a challenging task because of the multitude of different physical and chemical processes that are involved. Moreover, the nature of active sites for absorbents vary tremendously depending upon the source of the bioadsorbent, and the heterogeneous nature of functional groups in a single biosorbent makes it difficult to characterize them. It is encouraging that the modeling of single-component biosorption has been successful in validating the experimental data. However, in a practical scenario, the biosorption process is less likely to involve single-component adsorption. The biosorption of multiple components simultaneously on a heterogeneous biosorbent surface gives rise to complex and dynamic interactions among the metal ions and the functional groups. The key points for the modeling of the biosorption process are as follows:

(i) More complete mathematical models (2D with axial and radial dispersion) and computation techniques should be used to accurately model the complex physical and chemical phenomena.
(ii) Multicomponent biosorption modeling with respect to batch simulations is directly correlated to the concentration of all the species in the bulk phase in interaction with each specific functional group existing on the heterogeneous substrate and the availability of the interaction sites on the adsorbent. However, very few studies have been reported where the effect of process parameters on sorption efficiency has been studied though sensitivity analysis.
(iii) More experimental and modeling studies on the fixed-bed dynamics columns are needed to accurately predict performance on an industrial scale.
(iv) It is high time that the major focus of biosorption research shifts to pilot-scale studies with real wastewater rather than on laboratory experiments with metal solutions so that the technology can be practically applied. Research on the performance of the adsorbent materials is essential for the design of equipment employing the adsorption process.

(v) In a fixed-bed column, it is essential to characterize three different types of unknown parameters. In the first group are the ones that are experimentally obtained (i.e., mass of adsorbent, porosity). The ones that are determined according to correlations in the literature are considered to be in the second group. This includes parameters such as the atomic weight of cations. The third group is represented by parameters such as dispersivity, which are fitted from the breakthrough intervals.

Based on mathematical models, an appropriate numerical code can be compiled to validate the experimental data of both batch and fixed-bed columns. Further, the simulated data generated can be utilized in the prediction of steady state conditions and breakthrough time intervals in scaled-up batch and column tests, respectively. This manuscript has extensively focused on the complexity of biosorption research with respect to both the heterogeneity of the substrate and the presence of several interfering ions in the bulk phase. Recently, artificial neural networks (ANN) algorithms have been used to model such complex patterns. In others, the simulated data generated from discretized numerical schemes can be used as building blocks to generate future statistical data with ANN methods.

**Author Contributions:** Conceptualization, A.B.; Methodology, A.B.; Formal Analysis, A.B. and S.S.H.; Resources, A.B., S.S.A. and S.S.H.; Data Curation, A.B.; Writing—Original Draft Preparation, A.B.; Writing—Review & Editing, M.A., S.S.A. and S.S.H.; Visualization, S.S.A. and S.S.H.; Supervision, A.B. and M.A.; Project administration S.S.A. and S.S.H.; Funding Acquisition, A.B., S.S.A. and S.S.H. All authors have read and agreed to the published version of the manuscript.

**Funding:** This work was supported through the Annual Funding track by the Deanship of Scientific Research, Vice Presidency for Graduate Studies and Scientific Research, King Faisal University, Saudi Arabia [Project No. AN000121].

**Institutional Review Board Statement:** Not applicable.

**Informed Consent Statement:** Not applicable.

**Acknowledgments:** The authors acknowledge the Deanship of Scientific Research at King Faisal University for the financial support under the annual research project (No. AN000121).

**Conflicts of Interest:** The authors declare that there are no conflict of interest. All authors have seen and approved the manuscript being submitted. We warrant that the article is the authors' original work. We warrant that the article has not received prior publication and is not under consideration for publication elsewhere.

## References

1. Rani, L.; Kaushal, J.; Srivastav, A.L.; Mahajan, P. A critical review on recent developments in MOF adsorbents for the elimination of toxic heavy metals from aqueous solutions. *Environ. Sci. Pollut. Res.* **2020**, *27*, 44771–44796. [CrossRef] [PubMed]
2. Hanandeh, E.A.; Mahdi, Z.; Imtiaz, M.S. Modelling of the adsorption of Pb, Cu and Ni ions from single and multi-component aqueous solutions by date seed derived biochar: Comparison of six machine learning approaches. *Environ. Res.* **2021**, *192*, 110338. [CrossRef] [PubMed]
3. Güçoğlu, M.; Şatıroğlu, N. Adsorption of Pb(II), Cu(II), Cd(II), Ni(II), and Co(II) ions by newly synthesized 2-(2′-Hydroxyphenyl)Benzothiazole-functionalized silica. *J. Mol. Liq.* **2022**, *348*, 118388. [CrossRef]
4. Abass, M.R.; El-Kenany, W.M.; El-Masry, E.H. High efficient removal of lead(II) and cadmium(II) ions from multi-component aqueous solutions using polyacrylic acid acrylonitrile talc nanocomposite. *Environ. Sci. Pollut. Res.* **2022**, 1–17. [CrossRef]
5. Ramos, B.P.; Perez, I.D.; Aliprandini, P. $Cu^{2+}$, $Cr^{3+}$, and $Ni^{2+}$ in mono- and multi-component aqueous solution adsorbed in passion fruit peels in natura and physicochemically modified: A comparative approach. *Environ. Sci. Pollut. Res.* **2022**, 1–14. [CrossRef] [PubMed]
6. Mama, C.N.; Nwonu, D.C.; Akanno, C.C.; Chukwuemeka, O.E. Adsorption capacity of composite bio-modified geopolymer for multi-component heavy metal system: Optimisation, equilibrium and kinetics study. *Environ. Monit. Assess.* **2022**, *194*, 134. [CrossRef]
7. Spognardi, S.; Bravo, I.; Beni, C.; Menegoni, P.; Pietrelli, L.; Papetti, P. Arsenic accumulation in edible vegetables and health risk reduction by groundwater treatment using an adsorption process. *Environ. Sci. Pollut. Res.* **2019**, *26*, 32505–32516. [CrossRef]
8. Wei, Y.; Zhao, Y.; Zhao, X.; Gao, X.; Zheng, Y.; Zuo, H.; Wei, Z. Roles of different humin and heavy-metal resistant bacteria from composting on heavy metal removal. *Bioresour. Technol.* **2020**, *296*, 122375. [CrossRef]

9. Bayo, J.; Esteban, G.; Castillo, J. The use of native and protonated grapefruit biomass (*Citrus paradisi* L.) for cadmium(II) biosorption: Equilibrium and kinetic modelling. *Environ. Technol.* **2012**, *33*, 761–772. [CrossRef]
10. Ighalo, J.O.; Eletta, O.A.A. Recent advances in the biosorption of pollutants by fish scales: A mini-review. *Chem. Eng. Commun.* **2020**, *208*, 1301–1312. [CrossRef]
11. Naja, G.; Mustin, C.; Volesky, B.; Berthelin, J. Stabilization of the initial electrochemical potential for a metal-based potentiometric titration study of a biosorption process. *Chemosphere* **2006**, *62*, 163–170. [CrossRef] [PubMed]
12. Rahaman, M.S.; Basu, A.; Islam, M.R. The removal of As(III) and As(V) from aqueous solutions by waste materials. *Bioresour. Technol.* **2008**, *99*, 2815–2823. [CrossRef] [PubMed]
13. Xiao, Y.; Basu, A.; Kashyap, V.; Roberts, D.J. Experimental and Numerical Analysis of Biological Regeneration of Perchlorate Laden Ion-Exchange Resins in Batch Reactors. *Environ. Eng. Sci.* **2010**, *27*, 75–84. [CrossRef]
14. Yang, J.; Volesky, B. Cadmium Biosorption Rate in Protonated Sargassum Biomass. *Environ. Sci. Technol.* **1999**, *33*, 751–757. [CrossRef]
15. Bădescu, I.S.; Bulgariu, D.; Ahmad, I.; Bulgariu, L. Valorisation possibilities of exhausted biosorbents loaded with metal ions—A review. *J. Environ. Manag.* **2018**, *224*, 288–297. [CrossRef]
16. Ferreira, R.C.; Dias, D.; Fonseca, I.; Bernardo, M.; Willimann Pimenta, J.L.C.; Lapa, N.; de Barros, M.A.S.D. Multi-component adsorption study by using bone char: Modelling and removal mechanisms. *Environ. Technol.* **2022**, *43*, 789–804. [CrossRef]
17. Abdulaziz, M.; Musayev, S. Multicomponent Biosorption of Heavy Metals from Aqueous Solutions: A Review. *Pol. J. Environ. Stud.* **2017**, *26*, 1433–1441. [CrossRef]
18. Plazinski, W. Equilibrium and kinetic modeling of metal ion biosorption: On the ways of model generalization for the case of multicomponent systems. *Adsorption* **2013**, *19*, 659–666. [CrossRef]
19. Singh, S.; Kumar, V.; Datta, S.; Dhanjal, D.S.; Sharma, K.; Samuel, J.; Singh, J. Current advancement and future prospect of biosorbents for bioremediation. *Sci. Total Environ.* **2020**, *709*, 135895. [CrossRef]
20. Girish, C.R. Various isotherm models for multicomponent adsorption: A review. *Int. J. Civ. Eng. Technol.* **2017**, *8*, 80–86.
21. Basu, A.; Rahaman, M.S.; Islam, M.R. Extension of the pore diffusion approach for modelling binary adsorption of lead and arsenic ions in a fixed-bed column packed with atlantic cod fish scales. *Can. J. Chem. Eng.* **2011**, *89*, 499–507. [CrossRef]
22. Manjunath, S.V.; Kumar, M. Evaluation of single-component and multi-component adsorption of metronidazole, phosphate and nitrate on activated carbon from Prosopıs julıflora. *Chem. Eng. J.* **2018**, *346*, 525–534. [CrossRef]
23. Basu, A.; Rahaman, M.S.; Mustafiz, S.; Islam, M.R. Batch studies of lead adsorption from a multi-component aqueous solution onto Atlantic cod fish scale (Gadus morhua) substrate. *J. Environ. Eng. Sci.* **2007**, *6*, 455–462. [CrossRef]
24. Niu, C.H.; Volesky, B.; Cleiman, D. Biosorption of arsenic (V) with acid-washed crab shells. *Water Res.* **2007**, *41*, 2473–2478. [CrossRef] [PubMed]
25. Basu, A.; Mustafiz, S.; Islam, M.R.; Bjorndalen, N.; Rahaman, M.S.; Chaalal, O. A comprehensive approach for modeling sorption of lead and cobalt ions through fish scales as an adsorbent. *Chem. Eng. Commun.* **2006**, *193*, 580–605. [CrossRef]
26. Schiewer, S.; Volesky, B. Modeling Multi-Metal Ion Exchange in Biosorption. *Environ. Sci. Technol.* **1996**, *30*, 2921–2927. [CrossRef]
27. Assche, T.R.C.V.; Baron, G.; Denayer, J. An explicit multicomponent adsorption isotherm model: Accounting for the size-effect for components with Langmuir adsorption behavior. *Adsorption* **2018**, *24*, 517–530. [CrossRef]
28. Steffen, V.; Silva, E.A.; Evangelista, L.R.; Cardozo-Filho, L. Debye–Hückel approximation for simplification of ions adsorption equilibrium model based on Poisson–Boltzmann equation. *Surf. Interfaces* **2018**, *10*, 144–148. [CrossRef]
29. Patel, H. Fixed-bed column adsorption study: A comprehensive review. *Appl. Water Sci.* **2019**, *9*, 45. [CrossRef]
30. Danish, M.; Hashim, R.; Ibrahim, M.N.M.; Rafatullah, M.; Sulaiman, O. Surface characterization and comparative adsorption properties of Cr(VI) on pyrolysed adsorbents of Acacia mangium wood and *Phoenix dactylifera* L. stone carbon. *J. Anal. Appl. Pyrolysis* **2012**, *97*, 19–28. [CrossRef]
31. Hu, C.; Sedghi, S.; Madani, S.H.; Silvestre-Albero, A.; Sakamoto, H.; Kwong, P.; Pendleton, P.; Smernik, R.J.; Rodríguez-Reinoso, F.; Kaneko, K.; et al. Control of the pore size distribution and its spatial homogeneity in particulate activated carbon. *Carbon* **2014**, *78*, 113–120. [CrossRef]
32. Limousin, G.; Gaudet, J.P.; Charlet, L.; Szenknect, S.; Barthès, V.; Krimissa, M. Sorption isotherms: A review on physical bases, modeling and measurement. *Appl. Geochem.* **2007**, *22*, 249–275. [CrossRef]
33. Cunningham, J.A.; Werth, C.J.; Reinhard, M.; Roberts, P.V. Effects of grain-scale mass transfer on the transport of volatile organics through sediments: 1. Model development. *Water Resour. Res.* **1997**, *33*, 2713–2726. [CrossRef]
34. Saadi, R.; Saadi, Z.; Fazaeli, R.; Fard, N.E. Monolayer and multilayer adsorption isotherm models for sorption from aqueous media. *Korean J. Chem. Eng.* **2015**, *32*, 787–799. [CrossRef]
35. Nemeş, L.; Bulgariu, L. Optimization of process parameters for heavy metals biosorption onto mustard waste biomass. *Open Chem.* **2016**, *14*, 175–187. [CrossRef]
36. Ayawei, N.; Ebelegi, A.N.; Wankasi, D. Modelling and Interpretation of Adsorption Isotherms. *J. Chem.* **2017**, *2017*, 3039817. [CrossRef]
37. Çelebi, O.; Üzüm, Ç.; Shahwan, T.; Erten, H.N. A radiotracer study of the adsorption behavior of aqueous $Ba^{2+}$ ions on nanoparticles of zero-valent iron. *J. Hazard. Mater.* **2007**, *148*, 761–767. [CrossRef]
38. Vijayaraghavan, K.; Padmesh, T.V.N.; Palanivelu, K.; Velan, M. Biosorption of nickel(II) ions onto Sargassum wightii: Application of two-parameter and three-parameter isotherm models. *J. Hazard. Mater.* **2006**, *133*, 304–308. [CrossRef]

39. Brouers, F.; Al-Musawi, T.J. On the optimal use of isotherm models for the characterization of biosorption of lead onto algae. *J. Mol. Liq.* **2015**, *212*, 46–51. [CrossRef]
40. Rangabhashiyam, S.; Anu, N.; Giri Nandagopal, M.S.; Selvaraju, N. Relevance of isotherm models in biosorption of pollutants by agricultural byproducts. *J. Environ. Chem. Eng.* **2014**, *2*, 398–414. [CrossRef]
41. Foo, K.Y.; Hameed, B.H. Insights into the modeling of adsorption isotherm systems. *Chem. Eng. J.* **2010**, *156*, 2–10. [CrossRef]
42. Basu, A.; Islam, M.R. Scaling Up of Chemical Injection Experiments. *Pet. Sci. Technol.* **2009**, *27*, 654–665. [CrossRef]
43. Faust, S.D.; Aly, O.M. Adsorption Models. In *Adsorption Processes for Water Treatment*; Faust, S.D., Aly, O.M., Eds.; Butterworth-Heinemann: Oxford, UK, 1987; pp. 25–64. [CrossRef]
44. Li, H.; Yang, C. Nitrite Removal Using Ion Exchange Resin: Batch vs. Fixed Bed Performance. *Sep. Sci. Technol.* **2015**, *50*, 1721–1730. [CrossRef]
45. Ng, J.C.Y.; Cheung, W.H.; McKay, G. Equilibrium studies for the sorption of lead from effluents using chitosan. *Chemosphere* **2003**, *52*, 1021–1030. [CrossRef]
46. Nouri, L.; Ghodbane, I.; Hamdaoui, O.; Chiha, M. Batch sorption dynamics and equilibrium for the removal of cadmium ions from aqueous phase using wheat bran. *J. Hazard. Mater.* **2007**, *149*, 115–125. [CrossRef] [PubMed]
47. Ali Redha, A. Removal of heavy metals from aqueous media by biosorption. *Arab. J. Basic Appl. Sci.* **2020**, *27*, 183–193. [CrossRef]
48. Kaushal, A.; Singh, S. Adsorption phenomenon and its application in removal of lead from waste water: A review. *Int. J. Hydrol.* **2017**, *1*, 38–47. [CrossRef]
49. Ponnusami, V.; Rajan, K.S.; Srivastava, S.N. Application of film-pore diffusion model for methylene blue adsorption onto plant leaf powders. *Chem. Eng. J.* **2010**, *163*, 236–242. [CrossRef]
50. Weber, T.W.; Chakravorti, R.K. Pore and solid diffusion models for fixed-bed adsorbers. *AIChE J.* **1974**, *20*, 228–238. [CrossRef]
51. Saito, A.; Foley, H.C. Curvature and parametric sensitivity in models for adsorption in micropores. *AIChE J.* **1991**, *37*, 429–436. [CrossRef]
52. Baig, K.S.; Doan, H.D.; Wu, J. Multicomponent isotherms for biosorption of Ni2+ and Zn2+. *Desalination* **2009**, *249*, 429–439. [CrossRef]
53. Dissanayake, D.M.R.E.A.; Wijesinghe, W.M.K.E.H.; Iqbal, S.S.; Priyantha, N.; Iqbal, M.C.M. Isotherm and kinetic study on Ni(II) and Pb(II) biosorption by the fern *Asplenium nidus* L. *Ecol. Eng.* **2016**, *88*, 237–241. [CrossRef]
54. Ferreira, J.A.; Grassi, M.; Gudiño, E.; de Oliveira, P. A New Look To Non-Fickian Diffusion. *Appl. Math. Model.* **2015**, *39*, 194–204. [CrossRef]
55. Abdel-Ghani, N.T.; Hegazy, A.K.; El-Chaghaby, G.A. Typha domingensis leaf powder for decontamination of aluminium, iron, zinc and lead: Biosorption kinetics and equilibrium modeling. *Int. J. Environ. Sci. Technol.* **2009**, *6*, 243–248. [CrossRef]
56. Sari, A.A.; Amriani, F.; Muryanto, M.; Triwulandari, E.; Sudiyani, Y.; Barlianti, V.; Narrij Lotulung, P.D.; Hadibarata, T. Mechanism, adsorption kinetics and applications of carbonaceous adsorbents derived from black liquor sludge. *J. Taiwan Inst. Chem. Eng.* **2017**, *77*, 236–243. [CrossRef]
57. Ngah, W.S.W.; Hanafiah, M.A.K.M. Biosorption of copper ions from dilute aqueous solutions on base treatedrubber (Hevea brasiliensis) leaves powder: Kinetics, isotherm, and biosorption mechanisms. *J. Environ. Sci.* **2008**, *20*, 1168–1176. [CrossRef]
58. Vishan, I.; Saha, B.; Sivaprakasam, S.; Kalamdhad, A. Evaluation of Cd(II) biosorption in aqueous solution by using lyophilized biomass of novel bacterial strain Bacillus badius AK: Biosorption kinetics, thermodynamics and mechanism. *Environ. Technol. Innov.* **2019**, *14*, 100323. [CrossRef]
59. Du, J.; Sun, P.; Feng, Z.; Zhang, X.; Zhao, Y. The biosorption capacity of biochar for 4-bromodiphengl ether: Study of its kinetics, mechanism, and use as a carrier for immobilized bacteria. *Environ. Sci. Pollut. Res.* **2016**, *23*, 3770–3780. [CrossRef]
60. Lu, N.; Hu, T.; Zhai, Y.; Qin, H.; Aliyeva, J.; Zhang, H. Fungal cell with artificial metal container for heavy metals biosorption: Equilibrium, kinetics study and mechanisms analysis. *Environ. Res.* **2020**, *182*, 109061. [CrossRef]
61. Ali, M.H.; Hussian, A.M.; Abdel-Satar, A.M.; Goher, M.E.; Napiórkowska-Krzebietke, A.; El-Monem, A.M.A. The isotherm and kinetic studies of the biosorption of heavy metals by non-living cells of Chlorella vulgaris. *J. Elem.* **2016**, *21*, 1263–1276. [CrossRef]
62. Cui, H.; Yan, C.; Jia, P.; Cao, W. Adsorption and sensing behaviors of SF6 decomposed species on Ni-doped C3N monolayer: A first-principles study. *Appl. Surf. Sci.* **2020**, *512*, 145759. [CrossRef]
63. Mohan, D.; Singh, K.P. Single- and multi-component adsorption of cadmium and zinc using activated carbon derived from bagasse—an agricultural waste. *Water Res.* **2002**, *36*, 2304–2318. [CrossRef]
64. Torrik, E.; Soleimani, M.; Ravanchi, M.T. Application of Kinetic Models for Heavy Metal Adsorption in the Single and Multicomponent Adsorption System. *Int. J. Environ. Res.* **2019**, *13*, 813–828. [CrossRef]
65. Radke, C.J.; Prausnitz, J.M. Thermodynamics of multi-solute adsorption from dilute liquid solutions. *AIChE J.* **1972**, *18*, 761–768. [CrossRef]
66. Myers, A.L.; Prausnitz, J.M. Thermodynamics of mixed-gas adsorption. *AIChE J.* **1965**, *11*, 121–127. [CrossRef]
67. Jadhav, A.J.; Srivastava, V.C. Multicomponent adsorption isotherm modeling using thermodynamically inconsistent and consistent models. *AIChE J.* **2019**, *65*, e16727. [CrossRef]
68. Jadhav, A.J.; Srivastava, V.C. Adsorbed solution theory based modeling of binary adsorption of nitrobenzene, aniline and phenol onto granulated activated carbon. *Chem. Eng. J.* **2013**, *229*, 450–459. [CrossRef]
69. Noroozi, B.; Sorial, G.A. Applicable models for multi-component adsorption of dyes: A review. *J. Environ. Sci.* **2013**, *25*, 419–429. [CrossRef]

70. Xu, Z.; Cai, J.-G.; Pan, B.-C. Mathematically modeling fixed-bed adsorption in aqueous systems. *J. Zhejiang Univ. Sci. A* **2013**, *14*, 155–176. [CrossRef]
71. Karimi, S.; Tavakkoli Yaraki, M.; Karri, R.R. A comprehensive review of the adsorption mechanisms and factors influencing the adsorption process from the perspective of bioethanol dehydration. *Renew. Sustain. Energy Rev.* **2019**, *107*, 535–553. [CrossRef]
72. Lee, S.M.; Davis, A.P. Removal of cu(II) and cd(II) from aqueous solution by seafood processing waste sludge. *Water Res.* **2001**, *35*, 534–540. [CrossRef]
73. Chen, Q.; Tian, Y.; Li, P.; Yan, C.; Pang, Y.; Zheng, L.; Deng, H.; Zhou, W.; Meng, X. Study on Shale Adsorption Equation Based on Monolayer Adsorption, Multilayer Adsorption, and Capillary Condensation. *J. Chem.* **2017**, *2017*, 1496463. [CrossRef]
74. Mustafiz, S.; Basu, A.; Islam, M.R.; Dewaidar, A.; Chaalal, O. A Novel Method for Heavy Metal Removal. *Energy Sources* **2002**, *24*, 1043–1051. [CrossRef]
75. Ali, M.E.; Hoque, M.E.; Safdar Hossain, S.K.; Biswas, M.C. Nanoadsorbents for wastewater treatment: Next generation biotechnological solution. *Int. J. Environ. Sci. Technol.* **2020**, *17*, 4095–4132. [CrossRef]
76. Esalah, J.O.; Weber, M.E.; Vera, J.H. Removal of lead, cadmium and zinc from aqueous solutions by precipitation with sodium Di-(n-octyl) phosphinate. *Can. J. Chem. Eng.* **2000**, *78*, 948–954. [CrossRef]
77. Hayes, K.F.; Leckie, J.O. Modeling ionic strength effects on cation adsorption at hydrous oxide/solution interfaces. *J. Colloid Interface Sci.* **1987**, *115*, 564–572. [CrossRef]
78. Schiewer, S. Modelling complexation and electrostatic attraction in heavy metal biosorption by Sargassum biomass. *J. Appl. Phycol.* **1999**, *11*, 79–87. [CrossRef]
79. Yun, H.J.; Choi, Y.W.; Kim, N.J.; Sohn, D.W. Physicochemical properties of phosphatidylcholine (PC) monolayers with different alkyl chains, at the air/water interface. *Bull. Korean Chem. Soc.* **2003**, *24*, 377–383.
80. Hajahmadi, Z.; Younesi, H.; Bahramifar, N.; Khakpour, H.; Pirzadeh, K. Multicomponent isotherm for biosorption of Zn(II), CO(II) and Cd(II) from ternary mixture onto pretreated dried Aspergillus niger biomass. *Water Resour. Ind.* **2015**, *11*, 71–80. [CrossRef]
81. Hamdaoui, O.; Naffrechoux, E. Modeling of adsorption isotherms of phenol and chlorophenols onto granular activated carbon: Part I. Two-parameter models and equations allowing determination of thermodynamic parameters. *J. Hazard. Mater.* **2007**, *147*, 381–394. [CrossRef]
82. Walther, H.-J.; Buffle, J. Complexation Reactions in Aquatic Systems; Analytical Approach. *Acta Hydrochim. Hydrobiol.* **1989**, *17*, 230. [CrossRef]
83. Ofomaja, A.E.; Unuabonah, E.I.; Oladoja, N.A. Competitive modeling for the biosorptive removal of copper and lead ions from aqueous solution by Mansonia wood sawdust. *Bioresour. Technol.* **2010**, *101*, 3844–3852. [CrossRef] [PubMed]
84. McBride, M.B.; McBRIDE, M.B.A.; McBride, P.D.S.C.M.B. *Environmental Chemistry of Soils*; Oxford University Press: Oxford, UK, 1994.
85. Hikmat, N.A.; Qassim, B.B.; Khethi, M.T. Thermodynamic and Kinetic Studies of Lead Adsorption from Aquesous Solution onto Petiole and Fiber of Palm Tree. *Am. J. Chem.* **2014**, *4*, 116–124. [CrossRef]
86. Jena, P.R.; Basu, J.K.; De, S. A generalized shrinking core model for multicomponent batch adsorption processes. *Chem. Eng. J.* **2004**, *102*, 267–275. [CrossRef]
87. Nithya, K.; Sathish, A.; Kumar, P.S. Packed bed column optimization and modeling studies for removal of chromium ions using chemically modified Lantana camara adsorbent. *J. Water Process Eng.* **2020**, *33*, 101069. [CrossRef]
88. Milot, C.; McBrien, J.; Allen, S.; Guibal, E. Influence of physicochemical and structural characteristics of chitosan flakes on molybdate sorption. *J. Appl. Polym. Sci.* **1998**, *68*, 571–580. [CrossRef]
89. Kulkarni, R.M.; Vidya Shetty, K.; Srinikethan, G. Kinetic and equilibrium modeling of biosorption of nickel (II) and cadmium (II) on brewery sludge. *Water Sci. Technol.* **2019**, *79*, 888–894. [CrossRef]
90. Jeppu, G.P.; Clement, T.P. A modified Langmuir-Freundlich isotherm model for simulating pH-dependent adsorption effects. *J. Contam. Hydrol.* **2012**, *129–130*, 46–53. [CrossRef]
91. Nordstrand, J.; Dutta, J. Dynamic Langmuir Model: A Simpler Approach to Modeling Capacitive Deionization. *J. Phys. Chem. C* **2019**, *123*, 16479–16485. [CrossRef]
92. Xiao, B.; Thomas, K.M. Competitive Adsorption of Aqueous Metal Ions on an Oxidized Nanoporous Activated Carbon. *Langmuir* **2004**, *20*, 4566–4578. [CrossRef]
93. Keller, J.U.; Popernack, J.D.; Staudt, R. A generalization of langmuir′s adsorption isotherm to admolecules with interaction. In *Adsorption Science and Technology*; Hindawi: Brisbane, Australia, 2000; pp. 336–340. [CrossRef]
94. Wu, F.-C.; Liu, B.-L.; Wu, K.-T.; Tseng, R.-L. A new linear form analysis of Redlich–Peterson isotherm equation for the adsorptions of dyes. *Chem. Eng. J.* **2010**, *162*, 21–27. [CrossRef]
95. Kumar, K.V.; Monteiro de Castro, M.; Martinez-Escandell, M.; Molina-Sabio, M.; Rodriguez-Reinoso, F. A site energy distribution function from Toth isotherm for adsorption of gases on heterogeneous surfaces. *Phys. Chem. Chem. Phys.* **2011**, *13*, 5753–5759. [CrossRef] [PubMed]
96. Selim, H.M. Chapter Five—Transport and Retention of Heavy Metal in Soils: Competitive Sorption. In *Advances in Agronomy*; Sparks, D.L., Ed.; Academic Press: Cambridge, MA, USA, 2013; Volume 119, pp. 275–308.
97. Islam, M.A.; Chowdhury, M.A.; Mozumder, M.S.I.; Uddin, M.T. Langmuir Adsorption Kinetics in Liquid Media: Interface Reaction Model. *ACS Omega* **2021**, *6*, 14481–14492. [CrossRef] [PubMed]
98. Ucarli, O.; Yayintas, O.T.; Engin, M.S.; Cay, S.; Saglikoglu, G.; Yilmaz, S. Investigation of Competitive and Noncompetitive Adsorption of Some Heavy Metals Ions on Leucodon sciuroides (Hedw.) Schwägr. *Langmuir* **2020**, *36*, 8265–8271. [CrossRef] [PubMed]

99. Xiao, Y.; Azaiez, J.; Hill, J.M. Erroneous Application of Pseudo-Second-Order Adsorption Kinetics Model: Ignored Assumptions and Spurious Correlations. *Ind. Eng. Chem. Res.* **2018**, *57*, 2705–2709. [CrossRef]
100. Kumar, D.; Pandey, L.K.; Gaur, J.P. Metal sorption by algal biomass: From batch to continuous system. *Algal Res.* **2016**, *18*, 95–109. [CrossRef]
101. Yao, C.; Chen, T. A film-diffusion-based adsorption kinetic equation and its application. *Chem. Eng. Res. Des.* **2017**, *119*, 87–92. [CrossRef]
102. Song, F.Y.; Islam, M.R. Effect of salinity and rock type on sorption behavior of surfactants as applied in cleaning of petroleum contaminants. *J. Pet. Sci. Eng.* **1994**, *10*, 321–336. [CrossRef]
103. Sarwar, M.; Islam, M.R. A non-fickian surface excess model for chemical transport through fractured porous media. *Chem. Eng. Commun.* **1997**, *160*, 1–34. [CrossRef]
104. Rahman, M.H.; Wasiuddin, N.M.; Islam, M.R. Experimental and Numerical Modeling Studies of Arsenic Removal with Wood Ash from Aqueous Streams. *Can. J. Chem. Eng.* **2004**, *82*, 968–977. [CrossRef]
105. Ghorbani, F.; Younesi, H.; Ghasempouri, S.M.; Zinatizadeh, A.A.; Amini, M.; Daneshi, A. Application of response surface methodology for optimization of cadmium biosorption in an aqueous solution by Saccharomyces cerevisiae. *Chem. Eng. J.* **2008**, *145*, 267–275. [CrossRef]
106. Ho, Y.S.; McKay, G. Pseudo-second order model for sorption processes. *Process Biochem.* **1999**, *34*, 451–465. [CrossRef]
107. Alomá, I.; Martín-Lara, M.A.; Rodríguez, I.L.; Blázquez, G.; Calero, M. Removal of nickel (II) ions from aqueous solutions by biosorption on sugarcane bagasse. *J. Taiwan Inst. Chem. Eng.* **2012**, *43*, 275–281. [CrossRef]
108. Shafeeyan, M.S.; Wan Daud, W.M.A.; Shamiri, A. A review of mathematical modeling of fixed-bed columns for carbon dioxide adsorption. *Chem. Eng. Res. Des.* **2014**, *92*, 961–988. [CrossRef]
109. Yüksel, Ş.; Orhan, R. The Removal of Cr(VI) from Aqueous Solution by Activated Carbon Prepared from Apricot, Peach Stone and Almond Shell Mixture in a Fixed-Bed Column. *Arab. J. Sci. Eng.* **2019**, *44*, 5345–5357. [CrossRef]
110. Suzaki, P.Y.R.; Munaro, M.T.; Triques, C.C.; Kleinübing, S.J.; Fagundes Klen, M.R.; Bergamasco, R.; de Matos Jorge, L.M. Phenomenological mathematical modeling of heavy metal biosorption in fixed-bed columns. *Chem. Eng. J.* **2017**, *326*, 389–400. [CrossRef]
111. Amiri, M.J.; Khozaei, M.; Gil, A. Modification of the Thomas model for predicting unsymmetrical breakthrough curves using an adaptive neural-based fuzzy inference system. *J. Water Health* **2019**, *17*, 25–36. [CrossRef]
112. Lee, C.-G.; Kim, J.-H.; Kang, J.-K.; Kim, S.-B.; Park, S.-J.; Lee, S.-H.; Choi, J.-W. Comparative analysis of fixed-bed sorption models using phosphate breakthrough curves in slag filter media. *Desalination Water Treat.* **2015**, *55*, 1795–1805. [CrossRef]
113. Biswas, S.; Mishra, U. Continuous Fixed-Bed Column Study and Adsorption Modeling: Removal of Lead Ion from Aqueous Solution by Charcoal Originated from Chemical Carbonization of Rubber Wood Sawdust. *J. Chem.* **2015**, *2015*, 907379. [CrossRef]
114. Steiakakis, E.; Gamvroudis, C.; Alevizos, G. Kozeny-Carman Equation and Hydraulic Conductivity of Compacted Clayey Soils. *Geomaterials* **2012**, *2*, 37–41. [CrossRef]
115. Saadat, S.; Hekmatzadeh, A.A.; Karimi Jashni, A. Mathematical modeling of the Ni(II) removal from aqueous solutions onto pre-treated rice husk in fixed-bed columns: A comparison. *Desalination Water Treat.* **2016**, *57*, 16907–16918. [CrossRef]
116. Rahaman, M.S.; Omi, F.R.; Basu, A. Experimental and numerical modelling of arsenic adsorption in fixed-bed dynamic columns packed with atlantic cod fish scales. *Can. J. Chem. Eng.* **2015**, *93*, 2024–2030. [CrossRef]
117. Coskuner, G.; Bentsen, R.G. Prediction of Instability for Miscible Displacements in a Hele-Shaw Cell. *Oil Gas Sci. Technol.—Rev. IFP* **1987**, *42*, 151–162. [CrossRef]
118. Aksu, Z.; Çağatay, Ş.Ş.; Gönen, F. Continuous fixed bed biosorption of reactive dyes by dried Rhizopus arrhizus: Determination of column capacity. *J. Hazard. Mater.* **2007**, *143*, 362–371. [CrossRef] [PubMed]
119. Nwabanne, J.T.; Igbowe, P.K. Adsorption Performance of Packed Bed Column for the removal of Lead (ii) using oil Palm Fibre. *Int. J. Appl. Sci. Technol.* **2012**, *2*, 106–115.
120. Dawood, S.; Sen, T.K.; Phan, C. Performance and dynamic modelling of biochar and kaolin packed bed adsorption column for aqueous phase methylene blue (MB) dye removal. *Environ. Technol.* **2019**, *40*, 3762–3772. [CrossRef]
121. Charola, S.; Yadav, R.; Das, P.; Maiti, S. Fixed-bed adsorption of Reactive Orange 84 dye onto activated carbon prepared from empty cotton flower agro-waste. *Sustain. Environ. Res.* **2018**, *28*, 298–308. [CrossRef]
122. Lawson, S.; Adebayo, B.; Robinson, C.; Al-Naddaf, Q.; Rownaghi, A.A.; Rezaei, F. The effects of cell density and intrinsic porosity on structural properties and adsorption kinetics in 3D-printed zeolite monoliths. *Chem. Eng. Sci.* **2020**, *218*, 115564. [CrossRef]
123. Volesky, B. Biosorption process simulation tools. *Hydrometallurgy* **2003**, *71*, 179–190. [CrossRef]
124. Ali, M.A.; Islam, M.R. The Effect of Asphaltene Precipitation on Carbonate-Rock Permeability: An Experimental and Numerical Approach. *SPE Prod. Facil.* **1998**, *13*, 178–183. [CrossRef]
125. Ali, S.S.; Asif, M. Fluidization of nano-powders: Effect of flow pulsation. *Powder Technol.* **2012**, *225*, 86–92. [CrossRef]
126. Wakao, N. A Proposal of Calculational Model for Pressure Swing Adsorption Based on the Pore Diffusion. *J. Chem. Eng. Jpn.* **2001**, *34*, 1443–1448. [CrossRef]
127. Biesova, Z.; Miller, M.A.; Schneerson, R.; Shiloach, J.; Green, K.Y.; Robbins, J.B.; Keith, J.M. Preparation, characterization, and immunogenicity in mice of a recombinant influenza H5 hemagglutinin vaccine against the avian H5N1 A/Vietnam/1203/2004 influenza virus. *Vaccine* **2009**, *27*, 6234–6238. [CrossRef] [PubMed]